Optoelektronische Eigenschaften von π-konjugierten Polymeren

Dissertation

zur

Erlangung des Doktorgrades

der Naturwissenschaften

(Dr. rer. nat.)

dem

Fachbereich Chemie

der Philipps - Universität Marburg

vorgelegt von

Chan Im

aus Daejeon, Süd Korea

Marburg / Lahn 2002

Vom Fachbereich Chemie

der Philipps-Universität Marburg

als Dissertation am 10. Juni 2002 angenommen.

Erstgutachter : Prof. Dr. H. Bässler

Zweitgutachter : Prof. Dr. J. H. Wendorff

Tag der mündlichen Prüfung am 11. Juni 2002

Optoelectronic properties of π-conjugated polymers

Dissertation

Marburg, Germany 2002

Philipps University Marburg, Germany

Department of Chemistry

Institute of Physical, Macromolecular and Nuclear Chemistry

Chan Im

Republic of Korea

„Der Vogel kämpft sich aus dem Ei.

Das Ei ist die Welt.

Wer geboren werden will, muß eine Welt zerstören.

Der Vogel fliegt zu Gott.

Der Gott heißt Abraxas" [1]

You-Joung, Jung-Min,

und meinen Eltern

List of publications

C. Im, H. Bässler, H. Rost and H. H. Hörhold, **Hole transport in polyphenylene-vinylene-ether under bulk photoexcitation and sensitized injection**, J. Chem. Phys., vol. 113, no. 9, p. 3802, (2000).

C. Im, J. Lupton, P. Schouwink, S. Heun, H. Becker, and H. Bässler, **Fluorescence dynamics of phenylene substituted polyphenylenevinylene - trinitrofluorenone blend systems**, J. Chem. Phys., accepted, (2002).

C. Im, E. V. Emelianova, and H. Bässler, **Intrinsic and extrinsic charge carrier photogeneration in Phenylene substituted polyphenylenevinylene - trinitrofluorenone blend systems**, J. Chem. Phys., accepted, (2002).

D.P. West, M.D. Rahn, C. Im, H. Bässler, **Hole transport through chromophores in a photorefractive polymer composite based on poly n-vinylcarbazole**, Chem. Phys. Lett., vol. 326, p. 407, (2000).

S.C.J. Meskers, J. Hübner, M. Oestreich, C. Im and H. Bässler, **Relaxation of excitons and carge carriers in polymers**, IEEE Trans. Dielec. Elec. Insul., 8, p. 321, (2001).

J.P.J. Markham, T.D. Anthopoulos, I.D.W. Samuel, G.J. Richards, P.L. Burn, C. Im, and H. Bässler, **Non-dispersive hole transport in a spin-coated dendrimer film measured by the charge generation layer time of flight method**, Appl. Phys. Lett., submitted, (2002).

Conference participations

10th International Conference on Unconventional Photoactive Systems, Les Diablerets, Switzerland, September 4. - 8. 2001, C. Im, E. V. Emelianova, H. Becker, H. Spreitzer, and H. Bässler, **Intrinsic and extrinsic charge carrier photogeneration in phenyl-PPV: alkoxy substituted copolymeric poly-(para-phenylenevinylene) (poster)**

Deutsche Physiker Gesellschaft Frühjahrstagung, Symposium Organische Halbleiter, Regensburg, Germany, March 11. 2002, C. Im, E. V. Emelianova, P. Schouwink, J. Lupton, H. Bässler**, Fluorescence dynamics and charge carrier photogeneration of phenylene substituted polyphenylenevinylene - trinitrofluorenone blend systems (poster)**

Fifth International Symposium on Functional π-Electron Systems, Ulm/Neu-Ulm, Germany, May 2002, N. Schulte, T. Park, C. Im, H. Bässler, S.A. Haque, J.R. Durrant, R.J. Potter and A.B. Holmes, **New conjugated hole transport materials (poster)**

Fifth International Symposium on Functional π-Electron Systems, Ulm/Neu-Ulm, Germany, May 2002, W. Tian, C. Im, A. Fechtenkötter, M. Watson, K. Müllen, H. Spreitzer, H. Becker, and H. Bässler, **Charge carrier photogeneration in phenyl substituted poly-phenylenevinylene : perylene diimide and hexabenzo-coronene : perylene diimide blend systems (poster)**

Table of contents

1 Introduction

Why have π-conjugated polymers become so interesting and popular during the last decade? The answer lies in the fact that they have some significant advantage compared to conventional inorganic semiconducting materials. For example, easier processibility, low cost, flexibility, glass-quality, synthetical modifiablility, lightweight, and absorption and emission in visible light range. Therefore, they can be a very good candidate for proper optoelectronical active semiconducting materials for devices, e.g. rectifiers, photodiodes, light emitting diodes (LEDs) [2, 3], photovoltaic solar cells, [5] and field effect transistors[4]. Practically all plastic electronic devices are possible to produce.

They have already been successfully tested and used by many research groups and even by many companies. But there are still no real widespread products on the market because of some weaknesses regarding device stability, performance and lifetime etc. To overcome such problems, one should understand not only the qualitative device characteristics but also underlying mechanisms such as intrinsic photogeneration, transport, recombination and annihilation of charge carriers. The aim of this work is to understand those properties in a precise quantitative way.

This work is divided into five chapters as follows:

In the **first** chapter, general aspects of π-conjugated polymers are introduced. An overview of the π-conjugation, fundamental points about devices made of π-conjugated polymers and also theoretical background for this work will be briefly discussed.

In the **second** chapter, the excitation dynamics of the studied material, especially phenyl substituted copolymeric phenylenevinylene – trinitrofluorenone (TNF) will be discussed. To achieve this, a time-resolved fast photoluminescence technique, the so called, streak camera technique, is used and observed results will be discussed.

In the **third** chapter, the charge carrier photogeneration, using a method known as stationary photoconduction experiment, will be described and , subsequently, obtained results, which are mainly presented in a form of the charge carrier photogeneration quantum yield, will be presented and discussed as well.

In the **fourth** chapter, the charge carrier transport property of a π-conjugated polymer, which has an oxygen bridge between its repetition units, will be dealt with . The main method, the time-of-flight (TOF) technique, will be described and mobility results will be also discussed.

In the **last** chapter, all of the results will be summarized once again.

1.1 π-conjugated polymers

1.1.1 π-conjugation

It is well known that a bonding between carbons may not only be a single bond as in ethane (C_2H_6 – sp^3 hybrid orbital) but also double and even triple bond as in ethene (C_2H_4 – sp^2 hybrid orbital) and ethyne (C_2H_2 – sp^1 hybrid orbital), respectively. This fact is based on the electronic nature of carbon, which is explained by its ability of rearrangement, from its basic configuration $1s^2 2s^2 2p^2$ to the energitically favorable hybridized configurations as sp^3 or sp^2 configurations via mixing, to be more preciese, hybridizing of 2s and 2p orbitals.

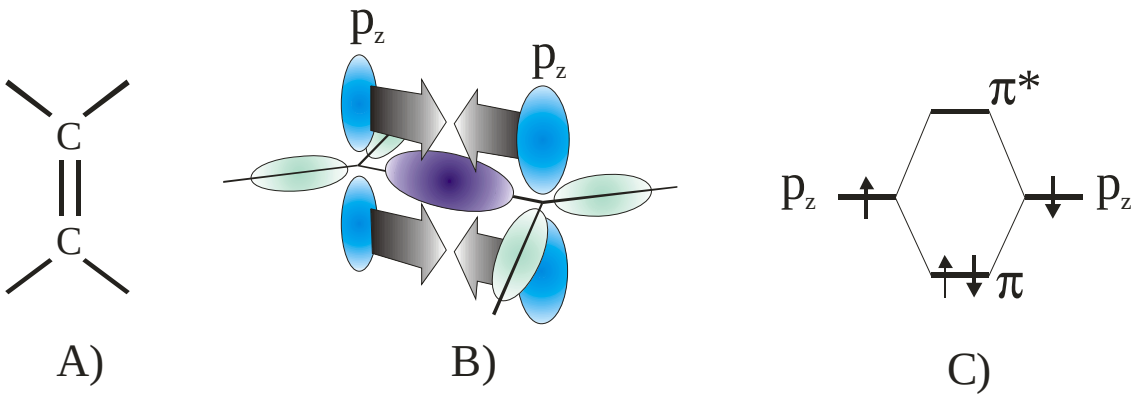

Figure 1 Scheme of σ- and π-bonding with two carbon atoms in ethene.

The Figure 1 shows schematic molecular orbitals of ethene and their energy level diagram. In the case of ethene, which has a double bond between carbon atoms, there are two different types of bonds known as σ-bond and π-bond. While the electron in the σ orbital is localized between two carbon atoms, the other electron in the π orbital is

more delocalized due to its parallel weak overlapping of p_z-atom orbitals. Therefore, the relatively weaker bound and delocalized electron within the π molecular orbital (MO) can be more easily contributed to the conductivity rather than the electron within the σ MO.

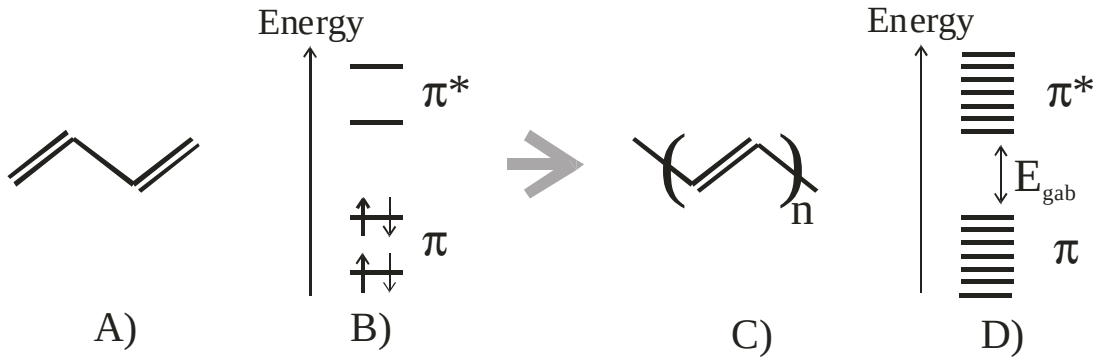

Figure 2 Scheme of trans-butadiene and poly acetylene, and their energy level diagrams.

By adding more carbons to C_2H_4, regularly alternated double and single bonds can be formed. The smallest example molecule is a 1,3-butadien as shown in Figure 2 A) (here, only a trans confirmational case) and the other more elongated example is a poly acetylene as shown in Figure 2 C). By increasing the number of the π-bonds alternatively, bonding and anti-bonding states are also increased and, consequently, the states are denser. At the same time, the splitting of both states, in other words, the energy gab between HOMO and LUMO will be closer. This regular and coplanar alternating of π bonding, i.e. conjugation, on which the π-electrons are delocalized, can provide extended conductivity, because π-electrons within the conjugation can be easily removed or added without breaking the molecular backbond in contrast to those electrons in σ MO, which are generally stronger localized. In the case of polyacetylene,

a Peierls distortion[6], which can affect the periodicity of the conjugation, can take place due to the energetically favorable dimerisation.

1.1.2 π-conjugated polymer solids

Aggregate states of π-conjugated polymers can be classified as follows. Firstly, an ideally isolated and relaxed polymer chain in vacuum, which is very often used for theoretical investigations, can be supposed. A more realistic situation is a solvated polymer chain in a dilute solution. More important aggregate states for optoelectronic applications are, of course, condensed solid states and one can divide such solids broadly into two classes as crystalline and amorphous states, according to their alignment situation. But although crystallized states have some advantages, for example, higher charge carrier mobility, they are not preferable to use because of difficulties during thin film preparations. Therefore, the most often used form is a glass type amorphous thin film which can be easily composited on to a substrate with a conventional low cost spin coating technique. Recently an ink-jet printing technique has also been used.

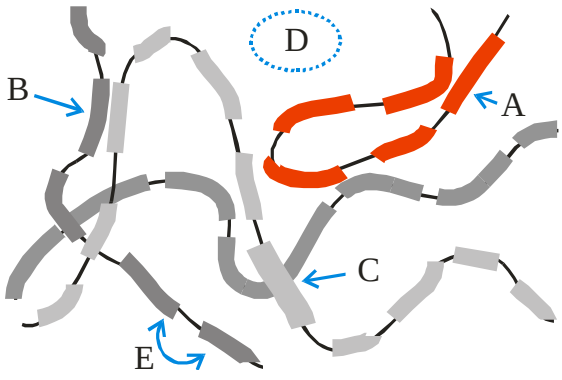

Figure 3 Schematic presentation of polymer chains in a amorphus solid.

In spite of the easier and flexibler preparation, condensed solids can cause some complications due to interchain processes because of their denser packing in addition to their intrachain interaction complexity. Typical issus, which are specific for such a condensed polymer solid systems, are, for instance, exciton diffusion, structural defects, change of effective conjugation length etc. Also one might have unexpected phase separations in blend systems.

In Figure 3 some possible interactions in condensed polyer solids are illustrated. Occasional neighboring of polymer chains (Figure 4 C) can cause interchain interaction. Such contact can also cause aligned parallel connection (Figure 4 B), in which both sites can interact more effectively, but such a locally ordered alignment can extended to form spatial crystalline domains or even extend to spread completely all over the sample. This interchain interaction might not be easily distinguished from an intrachain wide range interactions (Figure 4 A). Although an intrachain short range interactions is easier to recognise (Figure 4 E). Additionally, one should take into account a forming of empty spaces (Figure 4 D), which can affect percolative characteristic in hopping transport as well as increasing of internal surfaces.

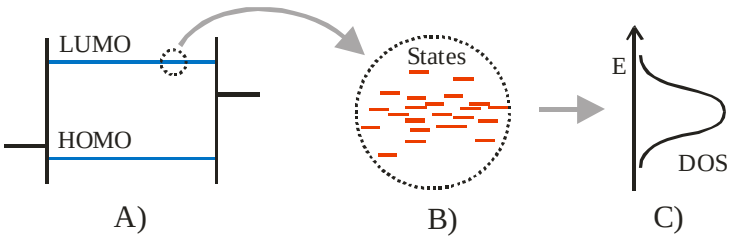

Figure 4 Schematic presentation of band structure and molecular picture.

With an microscopic understanding of a randomly disordered solid system as shown in Figure 3, one can imply a Gaussian type energytically distributed density of states (DOS) of HOMO and LUMO states, which is relevant for optoelectrical application, as in Figure 4 C). Figure 4 A) is a simplified 1-dimensional band structure representation of disordered systems being often used to describe conventional inorganic semiconductors. As one can see in Figure 4 B), optoelectronically active sites in a microscopic view are more isolated than band like structure in inorganic semiconductors because of their stronger molecular characteristics. It means that almost all phenomena in such a system is correlated with a diffusive relaxation and the time being needed for jumps. There is a very powerful tool, with which one can explore disordered solid systems like π-conjugated polymers. This disorder formalism was intensively developed by Bässler and his coworkers mainly using Monte Carlo simulation for hopping transport. In table 1 the most crucial differences between inorganic cristalline semiconductors and organic amorphous semiconductors are summarized.

In terms of the one-dimensional semiconductor model, developed by Su, Schrieffer, and Heeger [7, 8], the primary excitations are described as polarons and bipolarons generated on a time scale of less than 1 ps.[9] This model implies a weak Coulomb interaction between charged quasiparticles and pays very little attention to interchain and disorder effects. The molecular model of conjugated polymers [10, 11, 12], on the other hand, considers primary optical excitations as molecular excitons similar to those in oligomeric compounds. In this picture photoproduction of charge carriers is due to

dissociation of the excitons into Coulombically bound either on-chain [13, 14] or off-chain [61, 62] geminate pairs of elementary charges.

	Inorganic semiconductor	**Organic semiconductor**
Structure	Ordered - crystalline	Disordered - amorphous
Charges	Delocalized	Localized
Charge Transport	Non-dispersive $\mu > 1$ cm^2/Vs Field independent	Dispersive $\mu < 10^{-1}$ cm^2/Vs Field dependent
Exciton	Wannier type $E_b << kT$	Frenkel type $E_b b \sim 0.5$ eV $>> kT$

Table 1. A qualitative comparison between inorganic semiconductor and organic semiconductor

1.1.3 General concernings for devices

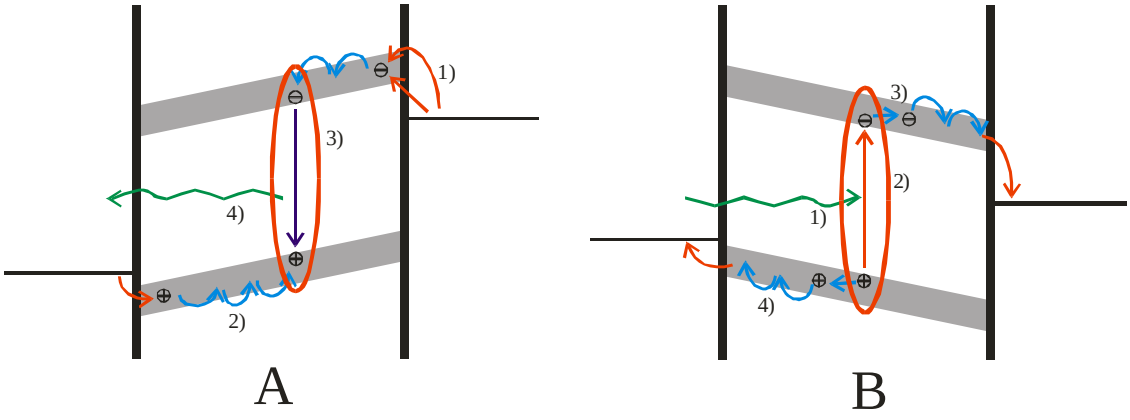

Figure 5 A: Schematic energy band diagram of a conventional organic LED, B: Schematic energy band diagram of a one layer organic photovoltaic cell.

Simple devices, consisting of π-conjugated thin film, are often sandwiched between semi-transparent indium tin oxide (ITO) and a metal electrode with a lower workfunction than an ITO electrode. As a typical example, two devices with their schematic functional mechanisms are shown in Figure 5. Although the case A) is for a light emitting diode (LED) and the other case B) is for a photovoltaic solar cell (PSC), they behave in a very similar manner except the functional direction due to their final purpose of usage. The former produce photons from injected electrons and holes, and the latter produce electrons and holes from absorbed photons.

The processes leading to electroluminescence in LED (case A) are: 1) electrons and holes injection, 2) hopping transport, 3) forming of excitations, and 4) radiative emission of photons. The processes to generate charge carriers in photovoltaic solar cell and also photodiode (case B) are: 1) photon absorption, 2) forming geminately bound e..h pairs, 3) dissociation to form free charge carriers, and 4) hopping transport to electrodes.

But as one knows, the difficulties in studing such devices is that one can not directly observe each property as a independent and individual process. In reality the processes strongly correlate with each other, therefore, this should be taken into account using a self-consistent method to investigate their quantitative analysis. Additionally, there are more problems: complicated interface behaviors, degradations, changing of morphology during operations, scattering or reflection of incident light or emission, impurity of materials, and etc.

1.2 Photo excitations in π-conjugated polymers

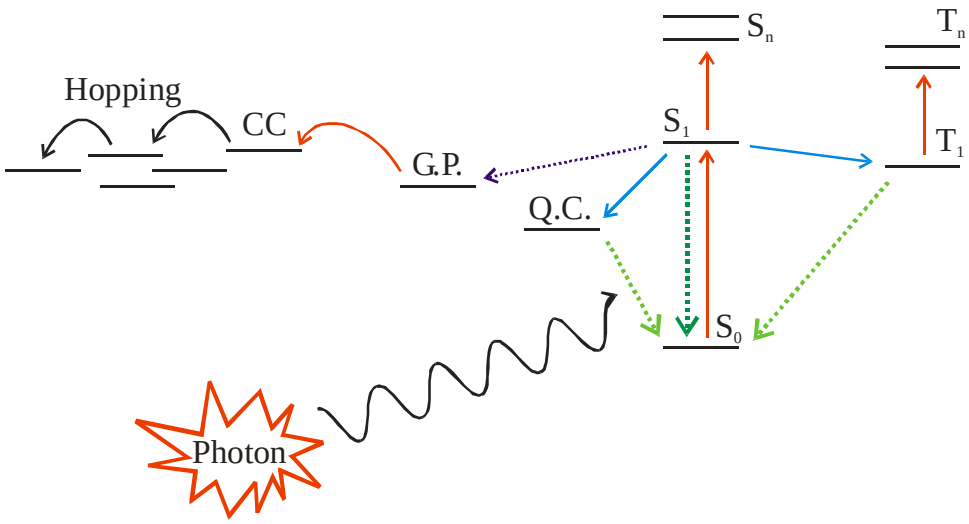

Figure 6 A Scheme for photoexcitation and relaxations of organic chromophore.

The above figure shows a brief diagram on the nature of excitations in common organic materials. A site or a chromophore on a oligomer or a polymer chain, which is found in a S_0 ground state, can absorb a photon and can subsequently form a S_1 excited state, but it can also form, with higher photon energy higher, excited states like S_2, S_3, and so on. And of course they are combined with vibronic states of their own electronic states. When excitations are formed, then they should dissipate to give their excess energy to the environment. In other words, they have to come back to their original relaxed state to reach a thermodynamically stable S_0 state through a favorable way. To return to the S_0 state, they may take various possible paths, which are competitive with each other, for instance, direct recombination to S_0 state radiatively or also non-radiatively, or inter system crossing transition from S_1 to T_1, or relaxation through chemical and/or physical

quenching centers. For charge carriers, the forming of metastable geminately bound e..h pairs, due to strong coulombic interaction, plays an important role.

This phenomena of excitation, especially in a solid of π-conjugated polymers, will be more complicated if one takes into account non-linear effects, such as singlet-singlet annihilation or triplet-triplet annihilation and also non-equilibrium behavior, similar to Förster transfer like relaxation of excitons in the DOS and geminate pair (GP) relaxation in a hopping motion. Such a non-linear or non-equilibrium phenomena are mainly caused by the condensed solid state phase of polymer molecules because of their close proximity to each other chromophores.

While the phenomenon of electroluminescence from organic, polymeric or small molecular light emitting diodes (LEDs) as well as the conceptual framework are basically understood, a quantitative assessment of the microscopic processes is still sparse. Among these microscopic processes are the kinetics of the recombination of electrons and holes injected from the electrodes and the pathways by which the generated excitations decay to the ground state.[15, 16] In a defect-free molecular system with balanced injection, sufficient to maintaining a stationary concentration of both electrons and holes of close to or even in excess of the capacitor charge, the electroluminescence is solely determined by the fraction of singlet excitations, or in the case of a phosphorescent emitter triplet excitations, multiplied by the intrinsic fluorescence yield and a geometric factor which accounts for optical losses due to wave guiding, internal reflection and reabsorption.[17, 18]

In a real world system there are inadvertently chemical and physical defects which can be populated by energy or charge transfer and which often catalyse non-radiative decay. In an LED, one would like to either eliminate these processes or exploit them via intelligent material design. It is obvious that improving the performance of organic LEDs requires a quantitative understanding of the kinetic processes involved in order to avoid harmful non-radiative decay.

Since the elementary process of energy and charge transfer among nearest and non-nearest neighbor chromophores occurs on a time scale of typically < 1 ps to several nanoseconds, fast fluorescence spectroscopy is the method of choice to characterize a given LED material.[19, 20]

Stationary and time resolved fluorescence was performed with neat PhPPV synthesized by Covion Organic Semiconductors GmbH and also with samples doped by various concentrations of trinitrofluorenone (TNF), known to be a strong electron acceptor. This material was chosen because of its high degree of chemical purity. By comparing the spectroscopic behavior of deliberately doped systems over an extended concentration range, we are able to delineate energy transfer to quantify the effect of charge accepting impurities and extrapolate to the behavior of an ideal system.

1.3 Charge carrier photogeneration

The origin of photoconductivity and charge carrier photogeneration in conjugated polymers has been extensively studied over the last decade but is still controversial as regarding both the nature of primary photoexcitations and the mechanism of carrier photoproduction.

There is abundant evidence in favor of the latter concept. By examining fluorescence and phosphorescence spectra of conjugated polymers it is known that there is an energy gap of roughly 0.7 eV between the lowest excited singlet level (S_1) and the first triplet level.[21, 22] This is unequivocal evidence for electron-electron exchange interaction in the excited state being significant. Recall that in a classic semiconductor, singlet and triplet states are degenerate. Independent theoretical as well as experimental results, also prove that the average electron hole separation in an optical excitation on a polymer, is of the order of 1 nm only[23, 24], albeit delocalized within a longer chain segment. Concomitantly, coulombic electron-hole attraction has got to be important and dissociation of the excitation must require a finite energy E_b. Unfortunately, there is no direct experiment to measure E_b in conjugated polymers directly because the oscillator strength for the transition from the ground state to the decoupled electron-hole pair state is vanishingly small, except for high quality polydiacetylene crystals. Employing the method of electro-reflection both the singlet exciton transition and the band to band transition have been measured in various polydiacetylene crystals and yield $E_b \sim 0.6$ eV.[25] Electron and hole injection from a surface tunneling tip confirmed that for

several non-crystalline conjugated polymers the single particle gap, i.e. the electrical gap, is about 0.5 eV higher than the optical gap.[26, 27]

On the other hand, it is a also well established fact that in conjugated polymers the photoconduction threshold is coincident with the absorption edge.[28 - 32] Although the photoconductive yield is much less than unity and strongly electric field dependent but weakly temperature dependent while the semiconductor band model suggest unit efficiency. Action spectra bear out a plateau within a photon energy range of up to almost 1 eV but increase strongly at higher energies. Obviously, some of the S_1 excitations are liable to subsequent dissociation although there the energy needed to overcome the coulombic attraction is not revealed in the temperature dependence. The so far unproven suspicion is that this process is aided by inadvertent dopants which act as sensitizers. By deliberate doping by an electron acceptor, trinitrofluorenone (TNF), the role of this mechanism will be examined and compared with electrode-sensitized photoinjection as well as intrinsic photoionization.[33]

Additionally, there is a well-established and also proven theory known as Onsager formalism for the charge carrier photogeneration and also for the recombination. This was originally publicated in 1938 to describe the dissociation probability of ion pairs under electric field. Today, this theory is successfully applied to a wide spectrum of systems, for example, amorphous Se, molecular crystals, polydiacetylene, etc.

In this formalism one can take into account themally activated diffusion, coulombic binding energy of e..h pairs, and the effect of external electric field to describe the

dissociation of geminately bound e..h pairs. Just one critical deficiency of this theory is that it does not explain how the initial distance will be estimated. Recently Arkhipov et al. have extended the 1-D and 3-D Onsager theory which is known as hot exciton on chain dissociation in order to explain ultrafast charge carrier photogeneration above the exciton binding energy level.

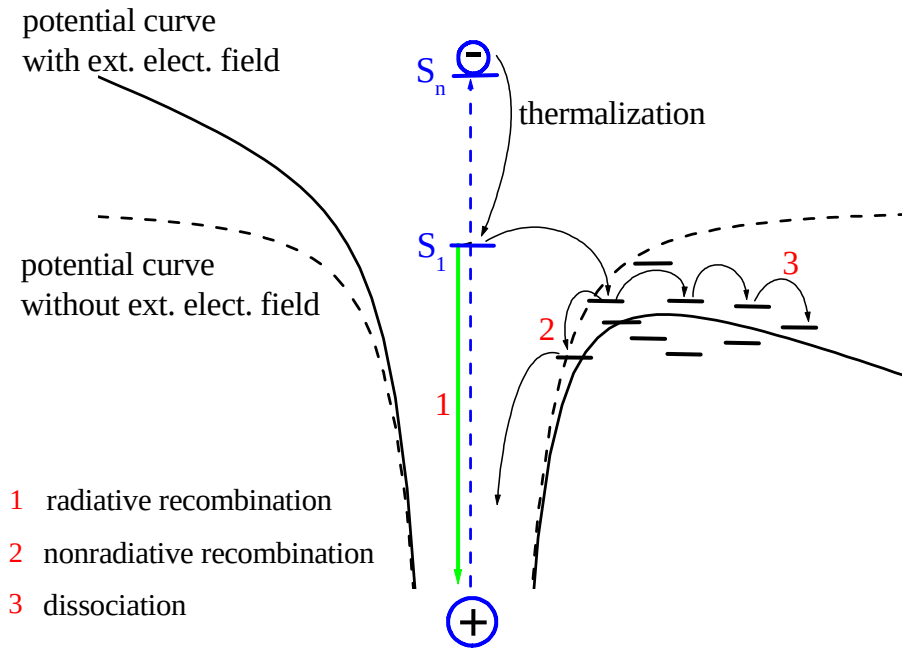

Figure 7 The Scheme of Onsager formalism for geminate pair dissociation and recombination

1.4 Charge carrier mobility

The charge carrier mobility is one of the most important material parameters in solid state devices in which excess charge carriers are generated by light or by dark injection from the electrodes. In electrophotography it is the transit time of a sheet of carriers across the sample which limits the time after which a latent image is formed. In a LED it determines the minimum response time of the device, although the actual response time is often set by the time needed to establish a critical charge reservoir rather than by the transit time of an individual charge carrier[34].

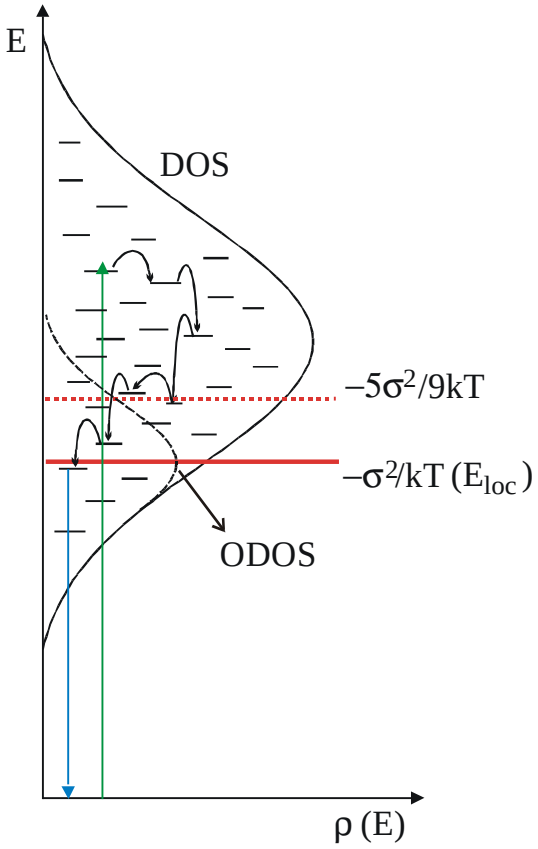

Figure 8 Gaussian density of states (DOS)

Meanwhile it is well accepted that in random organic solids, such as organic glasses or molecularly doped polymers, charge carriers move via hopping among neighbour molecules whose site energies are distributed because of local differences of the electronic polarization of a molecular radical anion and cation. The density of states distribution (DOS) is often of Gaussian form. Its counterpart is the inhomogenous absorption profile of a neutral chromophore in a glass[35]. The inhomogenity is due to local variations of the polarization energy of an excited molecules or a radical cation in a random matrix. Since it depends on an large number of internal coordinates, each varying randomly, the DOS will be of Gaussian shape[36]. Numerous studies of the temperature and field dependence of the charge carrier mobility, the influence on the presence of polar functionalities and the transition from non-dispersive to dispersive transport at decreasing temperature confirmed the validity of a transport model premised on the notion of disorder rather the polaron formation being of crucial importance[37].

The question which will be addressed in chapter 5 of this work is whether or not the disorder formalism is also applicable to conjugated polymers. Spectroscopically, they behave like an array of oligomers of statistically varying length, contributing to the inhomogenous broadening of excitonic transitions[38]. Therefore one might expect that charge transport is disorder controlled, the transport sites being identified as polymer segments. This is undoubtedly true as far as poly-phenylenevinylene (PPV) is concerned. It turned out that TOF signals are completely dispersive, not featuring a kink in time of flight (TOF) signals even plotted on double logarithmic scales[39].

At the other extreme, TOF signals measured with a film of ladder-type methyl substituted poly-(para-phenylene) (MeLPPP), which is by far the least disordered conjugated polymers as evidenced by its well structured absorption- and fluorescence spectra[40], are almost those of a molecular crystal. The dependence of the hole mobility on temperature and electric field is very weak although the absolute value of μ is a factor $\cong$ 300 less than that of crystalline anthracene.[41, 42] Therefore energetic disorder of polymers segments cannot be of key importance in this case. These are a few systems, though, which range in between, such as poly-(phenylphenylenevinylene) [43] , poly(1,4-phenylene-1,2-diphenoxphenylvinylene) (DPOP-PPV) [44], a phenylamino-substituted poly(phenylene-vinylene) (PAPPV) [42], poly-fluorene[45], and starburst phenylquinoxaline[46]. Relevant TOF signals do show a plateau indicative of Gaussian transport although broad tails indicate that disorder is important, as the $\ln \mu \propto F^{1/2}$ - type field dependence of μ. In order to get a deeper understanding of charge transport in that category of conjugated polymers we decided to look into the behavior of poly-phenylenevinylene ether (PPV-ether).

Another problem which will be addressed is related to the way charge carriers are produced in the course of a TOF experiment. Anticipating that in a disordered solid the distribution of jump rates is anomalously broad it does not mean that bulk photogeneration as compared to injection from a sensitizing generation layer[37] will yield identical TOF signals. In order to delineate any effect of the mode of photoinjection, TOF signals in PPV-ether are studied upon bulk excitation or upon photoexcitation in a thin rhodamine 6G generation layer. We will demonstrate that the mode of photoexcitaiton does have a profound influence on the degree of dispersion in

TOF signals while functional dependencies of the average transit time are similar. This lends further support to the concept of stochastic motion within an intrinsic distribution of hopping states for charge transport in conjugated polymers.

1.5 Materials

In this part, the materials investigated in this study will be presented.

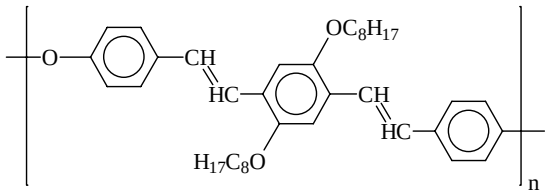

PPV-ether

Figure 9 Poly-para phenylenevinylene-ether (PPV-ether).

In Figure 9 a chemical structure of poly-paraphenylenevinylene-ether (PPV-ether) is shown. PPV-ether was provided by the research group of Prof. H.H. Hörhold, University Jena, Germany. This polymer has an oxygen-bridge between phenylenevinylene units. The advantage of such an ether-bridge is an effective restriction of the π-conjugation on the polymer chain in order to keep homogeneity.

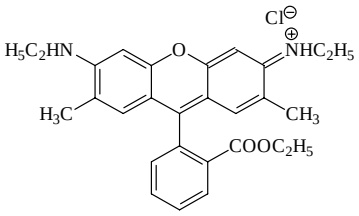

Figure 10 Rhodamine 6G (R6G).

The Rhodamine 6G (R6G) is a very efficient dye for laser application. This material was used mainly to composite a charge generation layer (CGL).

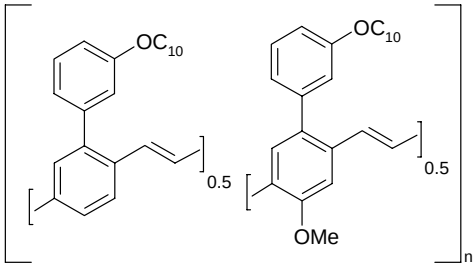

Figure 11 Phenyl substituted copolymeric PPV (PhPPV)

The second polymer is also a typical PPV derivative, which was synthesized via GILCH polymerizaton by COVION Organic Semiconductor GmbH.[63] The preferred object of the investigation is phenylene substituted polyphenylenevinylene manufactured by Covion Organic Semiconductor GmbH. Its high fluorescence yield suggests an exceptionally high degree of chemical purity.

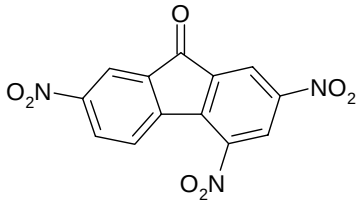

Figure 12 Trinitrofluorenone (TNF).

The trinitrofluorenone (TNF) was used as a very strong electron receptor due to its very high electron affinity, i.e. low lying LUMO level relative to that of active polymer.

2 Exciton dynamics

In this chapter, exciton dynamics of phenyl substituted polyphenylenevinylene (PhPPV), both in a pure neat film and also in films doped by electron accepting trinitrofluorenone (TNF), were discussed. Detail investigation of Exciton dynamics is important for the understanding of charge carrier photogeneration processes, as well as, for improving an electroluminescence performance of light emitting diodes (LEDs). Primary photoexcitation is known as an important source of free charge carriers whereas in case of LEDs a photoluminescence quantum yield is strongly affected by its lifetime. In reality both cases can easily vary their behaviors due to an existance of chemical and/or physical impurities.

A stationary photoluminescence spectroscopy and a time-resolved photoluminescence spectroscopy were employed to study exciton dynamics of PhPPV : TNF blend systems. A fast time-resolved spectroscopy within a nanoseconds range, generally known as a streak camera technique, was carried out with the collaboration of Dr. J.M. Lupton and Dr. P. Schouwink in the Max-Planck Institute for Polymer Reaserch in Mainz, Germany. The results in this chapter was publicated in J. Phys. Chem., 2002. (see publication list on page 4)

2.1 Experiment

2.1.1 Preparation

In the case of neat PhPPV, homogenous films with thicknesses of about 70 nm were spin-coated onto quartz substrates from 0.5 wt.-% toluene solutions. TNF was added as part of the total weight, for example, 1 % TNF doped polymer films were spin coated from a 0.495 wt.-% PhPPV / 0.005 wt.-% TNF solution in toluene. The film thickness was measured with Dektak surface profileometer.

2.1.2 Experimental methods

Steady-state photoluminescence spectroscopy was carried out with an excimer pumped dye-laser system (10 Hz repetition rate, 10 ns pulse width). The pulse energies could be tuned between 0.5 μJ and 50 μJ, dependent on the dye. Light emission was detected by an optical multichannel analyzer (OMA), which consisted of a 0.27 m monochromator in conjunction with a liquid-nitrogen cooled CCD camera (resolution 10 meV). The measurements were performed in a cold finger cryostat (10^{-4} mbar pressure) at approximately 80 K and 295 K.

For the time-resolved PL (TRPL) experiments a frequency doubled Ti:Sapphire laser producing 130 fs pulses at a repetition rate of 80 MHz, followed by a frequency doubling BBO crystal, was used to obtain the 435 nm excitation line. The detection system for the TRPL measurements consisted of a streak camera system with a maximal

time resolution of 2 ps, combined with a 0.25 m monochromator. TRPL measurements were carried out either at 4.2 K in a He static flow cryostat or at room temperature under vacuum (10^{-4} mbar pressure). In Figure 13 two sapmle spectra, which are measured at room temperature and 4 K, are shown.

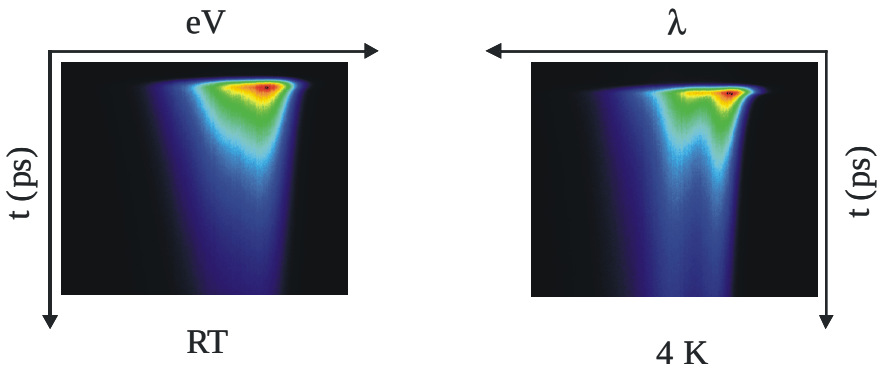

Figure 13 Example spectra measured with streak camera technique.

The PLE spectra were measured in a setup (Figure 14) that used a 150 W xenon-arc lamp as light source, followed by a 0.275 m monochromator. The light was chopped with a chopping rate of typically 30 Hz between the cryostat and the light source. A photomultiplier was used for both, detection of the excitation intensity and the PL signal intensity, with a lock-in amplifier (Stanford Research Systems, Model SR 850 DSP) which was connected to a chopper. The sample was kept in a liquid nitrogen cold finger cryostat at a temperature of 295 K under a vacuum of about 10^{-5} mbar during the PLE measurements. The relative PL quantum yield was calculated from the measured PL intensities taking into account corrections for the light source performance and the light absorption in the active areas of the films. Spectral dependencies of the corresponding

optical densities were measured with a Perkin-Elmer, Lambda 9 UV/VIS/NIR Spectrometer.

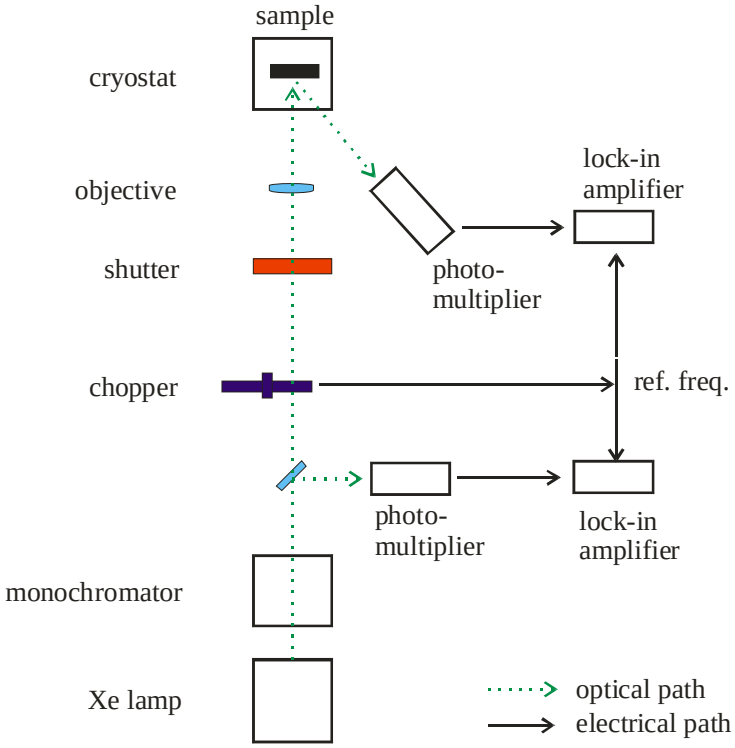

Figure 14 Schematic presentation of PLE setup

2.2 Results

2.2.1 PhPPV film

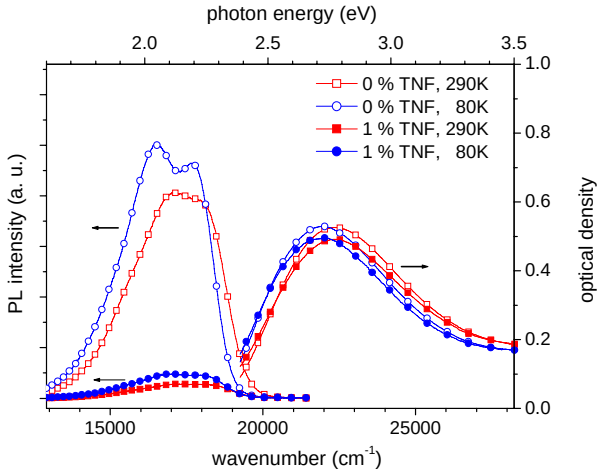

Figure 15 Steady state photoluminescence spectra and absorption spectra of spin coated films with and without TNF at 290 K and 80 K.

Figure 15 shows the 295 K and 80 K absorption and cw fluorescence spectra ($h\nu_{exc}$ = 2.76 eV) of both an undoped film and a film doped with 1 wt-% TNF. The absorption spectra reveal a minor bathochromic shift upon sample cooling, while any vibronic splitting is completely masked by large inhomogeneous line broadening. This implies that the variance of the Gaussian envelope of vibronic features is comparable to the dominant vibronic splitting, which is about 1400 cm^{-1}. Evidently, PhPPV is a conjugated polymer with a large degree of topologically controlled energetic disorder of the absorbing chromophores. On the other hand, the cw fluorescence spectra do reveal some vibronic splitting. The high energy emission tail ($S_1 \rightarrow S_0$ 0-0) corresponds to a

Gaussian with a width of about 600 cm^{-1}, i.e. half of the width of the inhomogeneously broadened absorption band. Such an effect is a well known phenomenon in conjugated polymers and indicates that the emissive singlet excitations accumulate at the lower portion of the density of state distribution (DOS).[49, 50] The absorption spectra of doped and undoped films are almost identical.

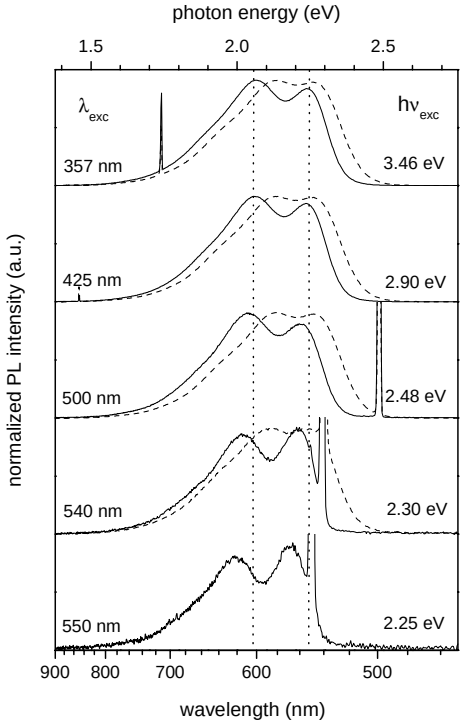

Figure 16 Steady state photoluminescence spectra recorded at 290 K (dashed line) and 80 K (solid line) at various excitation energies.

Upon recording the cw-fluorescence of an undoped PhPPV film at selected excitation energies, $h\nu_{exc}$, a change from spectrally invariant to quasi-resonant emission is observed. This change occurs whenever $h\nu_{exc}$ is below a certain critical localization energy below which an excitation is unlikely to undergo energy transfer to even lower energy sites before decaying. Remarkably, the spectrum excited at $h\nu_{exc}$ = 2.25 eV does

bear out a residual bathochromic shift, relative to that recorded at $h\nu_{exc}$ = 2.30 eV, which we attribute to a Stokes shift of ~ 170 cm^{-1}.(see Figure 16) This is a signature of moderate relaxation of the chain skeleton in the excited state, and indicates that the emission feature is, in fact, a phonon wing of a completely masked zero phonon transition in the terminology of molecular spectroscopy.[51]

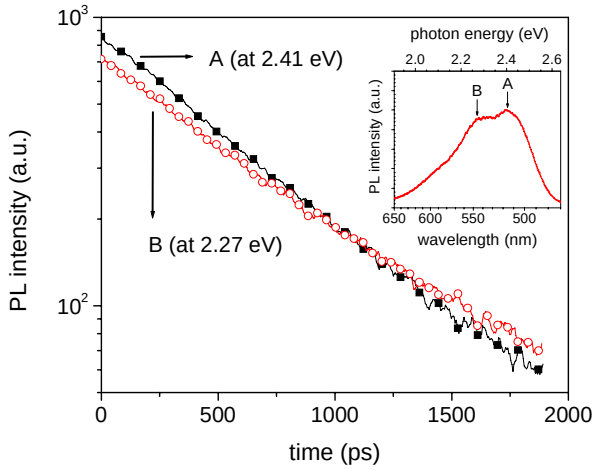

Figure 17 Transient photoluminescence of PhPPV/MTHF in dilute solution at 295 K. Filled and opened symbols refer to probing at spectral positions A and B in inset respectively.

Next we measured the fluorescence decay of PhPPV in solution at 295 K excited at 3.10 eV (400 nm) and probed at 2.41eV (18200 cm^{-1}) and 2.27 eV (16800 cm^{-1}), i.e. at the maxima of the $S_1 \rightarrow S_0$ 0-0 transition and the dominant first vibronic band which, in fact, is a convolution of several vibronic features associated with the phenylenevinylene group (see inset to Figure 17). It turns out that both decay functions are monoexponential, but with slightly different lifetimes of 650 ps and 750 ps, and that therefore the low energy emission band grows relative to the high energy band. This implies that there is a superposition of two emissions with slightly different decay times,

most likely differing regarding the strength of vibronic coupling only. In Figure 17 and in the following figures pertaining to fluorescence decay the temporal evolution of the fluorescence will be plotted on a double logarithmic ln (I_0 / I(t)) vs. log t-scale appropriate for testing a stretched exponential, i.e. a Kohlrausch-Williams-Watts-type (KWW) decay function [52]

$$I(t) = I_0 \exp[-(t/\tau_0)^{\beta}], \qquad 0 < \beta < 1 \qquad (1).$$

On such a scale a simple exponential decay with $\beta = 1$ reproduces a straight line with unit slope while $\beta < 1$ indicates that there is a distribution of decay times. τ_0 is the time at which the intensity is reduced to 1/e of its maximum value. The data from Figure 17 confirm that the decays from both emissive states of PhPPV are almost exponential yielding decay times of 650 ps and 750 ps, respectively. Presuming that the radiative decay is the same of that of a oligomeric PV with 3 phenylene rings, namely 1.12 ns [53], one arrives at an approximate fluorescence yield $\eta_0^{PhPPV} \sim 0.6$.

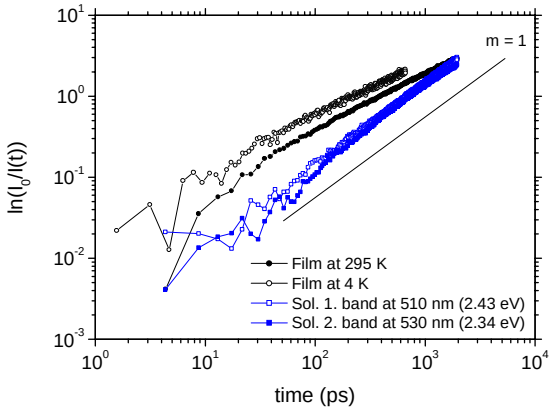

Figure 18 KWW-type plots of neat PhPPV and dilute PhPPV/MTHF solution.

It is informative to compare the spectrally integrated decays of the fluorescence from a neat PhPPV film recorded at 295 K and at 4.2 K. Data shown in Figure 18 indicate that (i) the decay is exponential only at short times and approaches a KWW-type decay with $\beta = 0.7$ yielding a 1/e decay time of ~ 400 ps, and (ii) upon cooling to 4.2 K the decay becomes a factor of 2 faster though retaining the functional dependence.

By calculating the integrals $\int_0^{2\,ns} I(t)\,dt$ for fluorescence from solution and film at 295 K, respectively, one finds that $\eta^{film} / \eta^{sol} \sim 0.7$. Adopting the above value $\eta_0^{PhPPV} \sim 0.6$, one arrives at a fluorescence quantum yield within the film of $\eta^{film} \sim 0.4$. The fact that there is merely a 30 % loss of fluorescence yield upon going from solution to film is a signature of the high degree of purity of the material.

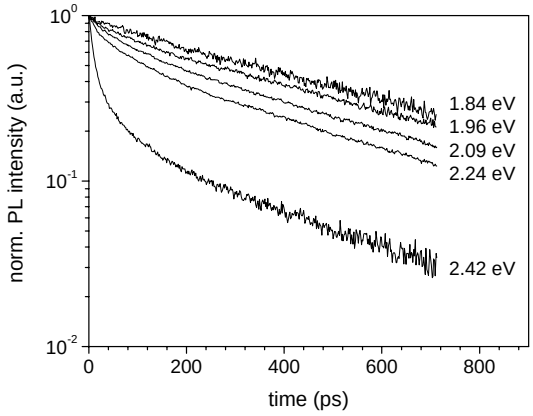

Figure 19 Decay of the photoluminescence from a neat PhPPV film probed at selected emission energies.

It is also informative to plot the fluorescence decay of selected narrow spectral detection windows as shown in Figure 19. Evidently the fluorescence decay is not uniform across the emission spectrum. The higher the emission energy is, the faster the intensity decays.

This illustrates the effect of spectral diffusion within a down manifold of inhomogeneously broadened chromophores.

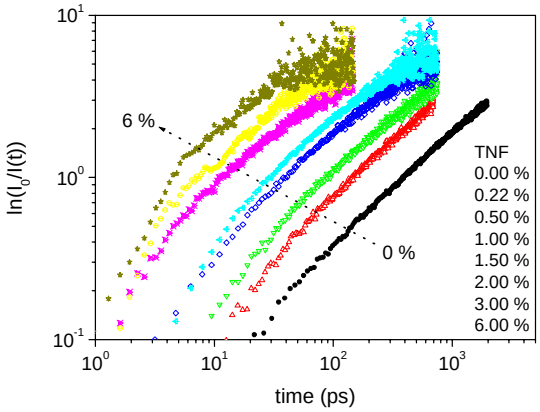

Figure 20 KWW plots for PhPPV films with various TNF concentrations.

2.2.2 PhPPV doped with TNF

As expected the fluorescence from a PhPPV film decays more rapidly as TNF is added. Since the absorption spectrum of TNF does not overlap with the emission spectrum of PhPPV, the quenching of the PhPPV singlet excitation must be due to electron transfer from the singlet excitation rather than due to energy transfer [54]. The generated electron-hole pair, i.e. charge transfer state, must decay non-radiatively because the energy of a geminate $(PhPPV)^+$ and $(TNF)^-$ pair is insufficient to generate an emissive state. Figure 20 shows a family of KWW plots parametric in dopant concentration. It is noteworthy that on a log ln (I_0 / I(t)) vs. log t-scale the decay pattern is merely shifted along the abscissa maintaining its functional character except for a marginal change of β from $\cong$ 0.7 at the lowest concentration (0.22 %) to $\cong$ 0.6 at higher concentration. Remarkably, the KWW-plot for the undoped film features the same decay law.

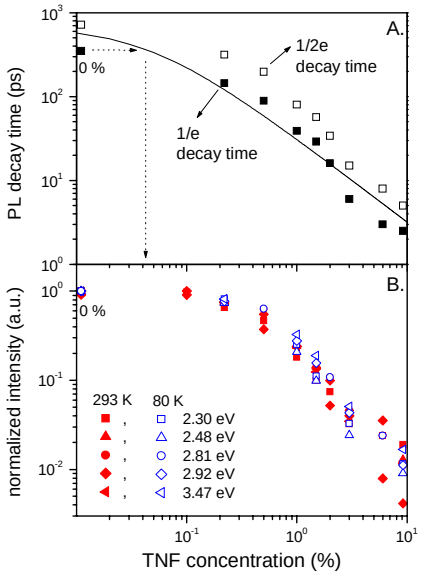

Figure 21 A: TNF concentration dependences of PL decay time as 1/e (full rectangle) and 1/2e (open rectangle) B: TNF concentration dependences of cw-PL intensity at 295K and 80K with various excitation energies. The solid line was calculated from the eq. 3 using τ_0 of 0.7 ns and k_t of 3.18 x 10^{12} s^{-1}.

In Figure 21A the 1/e decay times as well as the 1/2e decay times are shown as a function of concentration. The former bears out a linear law while the latter approaches a $c^{-1.3}$ dependence at large concentration and concurs with the drop of the steady state fluorescence intensity as the concentration increases (Figure 21B).

Upon recording the cw-fluorescence spectra as a function of TNF concentration renders a continuous hypsochromic shift with increasing concentration (Figure 22A). It is matched by an analogous bathochromic shift in the time-resolved spectra upon shifting the temporal detection window to later times (Figure 22B). As will be shown later, both phenomena are related and can be attributed in the spectral diffusion of the PhPPV singlet excitation. The data analysis will be shown in the discussion section.

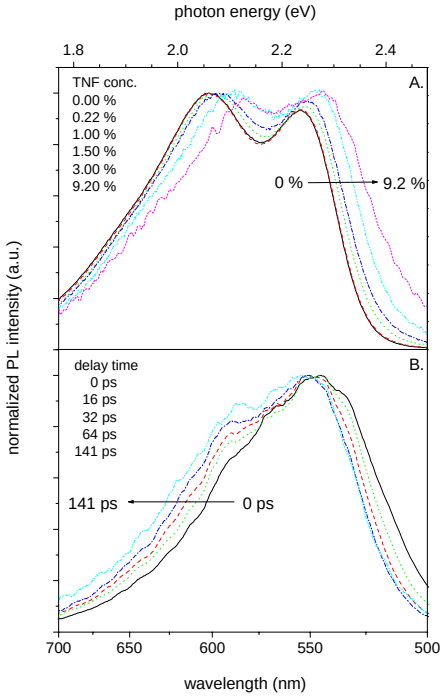

Figure 22 A.: cw-photoluminescence spectra of neat PhPPV film at 80 K (λ_{exc} = 425 nm), B.: time resolved photoluminescence spectra of neat PhPPV at 290 K (λ_{exc} = 430 nm)

2.2.3 Photoluminescence excitation spectroscopy

In order to find out whether or not quenching of singlet excitations is facilitated by the excess energy of the initially generated Franck Condon State, the photoluminescence excitation (PLE) spectra for undoped and doped PhPPV were measured. To measure the PLE yield quantitatively is notoriously difficult, because of the need to assess the relative contributions of internal and external reflection losses.

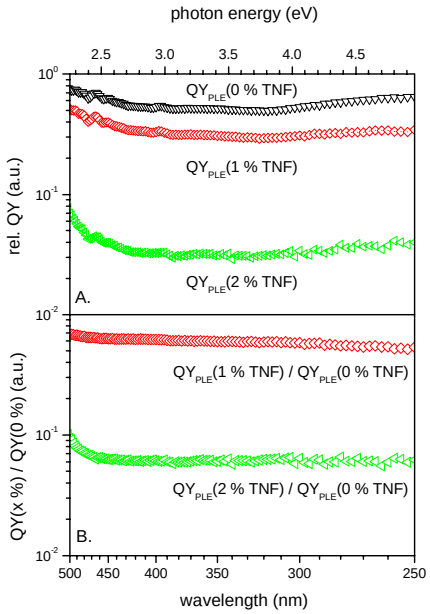

Figure 23 PLE spectrum with various TNF concentration.

However, from the results in Figure 23A, the PLE yield of the undoped film can safely be considered to be constant over the entire spectral range studied (Figure 23B). Thus, normalizing the PLE spectrum of a PhPPV film doped with 6 % of TNF to that of the undoped film removes any ambiguity in this respect (Figure 23B). The result included in Figure 23 proves that singlet quenching via electron transfer towards TNF proceeds exclusively from the relaxed state. The only effect observed is the increase of the PLE yield in the doped sample in the long wavelength tail of the absorption spectrum. This is due to excitations which are immobilised at tail states within the density of states distribution and are, therefore, less liable to charge transfer towards a dopant molecule.

2.3 Discussion

2.3.1 Fluorescence

The main results in this chapter of fluorescence decay are that (i) the fluorescence from PhPPV in solution decays exponentially, (ii) in a neat film it is exponential only at short times and approaches a stretched exponential, i.e. KWW law, at longer times, and (iii) doping a PhPPV film with TNF accelerates the fluorescence decay but the functional pattern is preserved.

A stretched exponential behavior is an indication that the excitations are removed from the ensemble of potentially emissive states and, notably, that the process is not controlled by a well defined transfer rate but rather by a distribution of rates. The underlying process could be either of a parallel or a serial type. A text book example for the parallel type is Förster type, resonant dipole-dipole mediated energy transfer in which a given excited donor molecule interacts with a spatially random array of absorbers. It leads to a stretched exponential with $\beta = ½$.[55] The serial type can be described as a consecutive series of donor-donor transfer steps that ultimately leads to excited state quenching and where excitation transport towards the quencher is the rate limiting step. However, for shorter times KWW plots must extrapolate to a mono-exponential decay because there must be a minimum transfer time between nearest neighbor chromophores. The situation becomes more complicated if the acceptor state is fluorescent, in which case the emission can approach an exponential decay law at longer times as well.

The fact that the KWW-plots of the fluorescence from both doped and undoped PhPPV films approach a straight line behavior with $\beta = 0.65 \pm 0.05$ while the fluorescence decay from an isolated PhPPV chain in solution is exponential leads to several conclusions. Firstly, it confirms that quenching of PhPPV singlet excitations in the doped film is not due to Förster-type energy transfer but, rather, due to intra- as well as inter-chain transport which ultimately leads to the formation of a $(TNF)^-$ and $(PhPPV)^+$ geminate pair via short range electron transfer. It is important, though, to recognize that the same functional KWW dependence is observed with undoped PhPPV films. It implies that it is also determined by a small yet finite concentration of charge acceptors of unidentified origin which quench singlet excitons. They may either be inadvertent chemical impurities or physical dimers at which the coulombic binding energy of an e..h pair exceeds the energy of an on-chain singlet state. The existence of impurities and defects has firmly been established via thermally stimulated photoluminescence and from photoconductivity near the absorption edge.[56] The ubiquitous observation that the fluorescence from films of conjugated polymers usually deviates from a single exponential law has, therefore, a simple explanation. Consequentially, extrapolating the long time fluorescence decay of a conjugated polymer film in a semi-logarithmic plot would over-estimate the intrinsic life time.

2.3.2 Kinetic analysis

The operationally simplest way to quantify the doping effect on the fluorescence in PhPPV is to plot experimentally determined 1/e decay times as a function of

concentration. On a short time scale one can neglect the time dependence of the rate constant k_t of singlet exciton quenching via electron transfer to TNF present at a concentration c expressed in mole/mole units. Since the molecular weights of TNF and the polymer repeat units are similar and expressing the concentration via the weight percentage makes no difference, one can adopt a simple kinetic scheme for singlet excitations

$$\frac{d[s]}{dt} = -(k_0 + k_t \cdot c) \cdot [s] \qquad (2)$$

where $\tau_0 = k_0^{-1}$ is the intrinsic life time including intra-chain non-radiative decay

$$\tau_e = (k_0 + k_t \cdot c)^{-1} \qquad (3),$$

is the time after which the intensity has decayed to 1/e of the initial value. For an average life time of the isolated chain of 0.7 ns, $k_t = 3.2 \times 10^{12}$ s^{-1} is obtained for a TNF concentration of 0.22 % and an 1/e decay time of 144 ps. Regarding the value of k_t one should recognize that in a conjugated polymer a chromophore of the polymer is composed of several repeat units and, therefore, the quenching effect by a dopant molecule is enhanced relative to that of a solid made up by small molecules. By plotting τ_e versus concentration in terms of eq (3), one can estimate the concentration of inadvertent singlet quenchers in “neat” PhPPV, which are responsible for the reduction in singlet lifetime in films with respect to isolated chains, to be ≤ 0.04 % by weight.

If one considers excitation quenching by dopants on a longer time scale, one has to bear in mind that excitation transport is a stochastic non-equilibrium, i.e. dispersive process. This can formally be accounted for by a time dependence of the ensemble-averaged momentary hopping rate of the form

$$k(t) = \nu_0 (t / t_0)^{\alpha - 1} \qquad (4)$$

where ν_0 and t_0 are the jump frequency and jumping time in an energetically discrete hopping system and α is the dispersion parameter.[57] Therefore eq. (1) has to be replaced by

$$\frac{d[s]}{dt} = -(k_0 + k(t) \cdot c) \cdot d[s],$$

giving

$$[s](t) = [s]_0 \exp - \left[k_0 \cdot t + c \cdot \int_{t_0}^{t} k(t') \cdot dt' \right] \qquad (5)$$

The integral in the exponent in eq. (5) is the time averaged hopping rate within the time domain in which excitation quenching occurs. It depends on the dopant concentration. Because time and, concomitantly, concentration enter the upper bound of the integral it cannot be calculated analytically. Qualitatively, however, the consequence is straightforward. Since according to eq. (4) the hopping motion of singlet excitations towards the dopant is retarded as time proceeds, the time averaged hopping rate must increase as the concentration increases. Therefore the time averaged survival probability of PhPPV excitations must decay faster than eq. (1) predicts. This is borne out by fig. 8 which indicates that at high concentration I(c) follows a $I(c) \sim c^{-1.3}$ law instead of a linear law.

2.3.3 Kohlrausch-Williams-Watt analysis

There is further useful information which can be extracted from a KWW-type analysis of fluorescence decays. Fluorescence decays as discussed above refer to spectrally non-

selective decay. The experiments therefore monitor the survival probability of intrinsic PhPPV excitations with respect to their hopping motion within the manifold of intrinsic hopping states. On the other hand, if one measures the fluorescence decay within a spectrally narrow detection window, as shown in Figure 19, one counts all excitations entering and leaving a well defined energy slice of the distribution of hopping states. Therefore one monitors depletion of the reservoir of singlet excitations by spectral diffusion of excitations and excited state depletion due to quenching. It was shown above (see Figure 20) that the fluorescence decay from doped PhPPV is due to sequential transport towards the dopant and leads to a KWW exponent of $\beta = 0.65 \pm 0.05$. However, the fluorescence decay in a neat PhPPV film recorded within an energy slice of 0.2 eV centered at 2.42 eV, i.e. at the high energy wing of the $S_1 \rightarrow S_0$ $0 \rightarrow 0$ fluorescence band, is different. It does approach a KWW pattern but with a final slope of $\beta = 0.34$ (Figure 24).

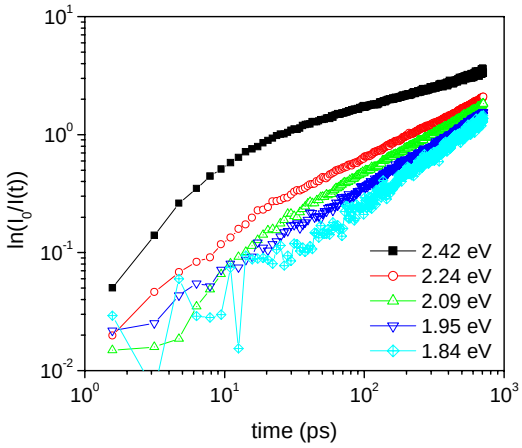

Figure 24 KWW-type plots for neat PhPPV at various detection energy (data from Figure 19).

It proves that within this energy range of excitation the decay kinetics are governed mainly by excitations leaving the detection window by migrating towards the tail of the DOS via Förster-type energy transfer rather than via quenching by dopants. This behaviour is both in agreement with the Monte Carlo master equation hybrid technique using a self-avoiding random walk algorithm[58] and with earlier related experimental work on a ladder-type poly-phenylene.[59] Upon shifting the detection window towards lower energies the KWW exponent β increases and approaches the value 0.65 ± 0.05 indicating that in this spectral range spectral diffusion has come to an end and most of the fluorescence loss processes are due to a combination of dissociative quenching and intrinsic decay.

2.3.4 Spectral diffusion

The bathochromic shift of the gated fluorescence spectra of PhPPV as a function of delay time relative to the exciting laser pulse is an unambiguous signature of spectral diffusion. It occurs when a chromophore in a bulk system is optically excited, unless this excitation occurs in the tail of the density of state distribution where the excitations are already localized. It is caused by energy transfer towards lower lying states and has been dealt with at length, both theoretically and experimentally. From the work by Movaghar et al.[60], it is known that the mean energy of the excitation decreases on an approximately logarithmic scale. In the long time limit the ensemble of excitations tends to approach quasi-equilibrium. However, if the excitations are singlets with an intrinsic life time of ~ 1 ns only, quasi-equilibrium will hardly ever be attained and most excitations end their lives near the so-called localization edge. Excitations that are

created below that threshold are, on average, not affected by spectral diffusion and decay from their original chromophore, as testified by [60].

The data of Figure 21B are in full accordance with this concept, and the experimental transient fluorescence spectra recorded within a narrow time window as a function of the delay time can be mapped. In Figure 25, the center of the $S_1 \rightarrow S_0$ 0-0 emission energy is plotted on a logarithmic time axis. Analysing the data in terms of the theory by Movaghar et al.[60] yields a Gaussian width of $\sigma \sim 0.125$ eV for the DOS and the minimum time τ_{min} required for a downward jumps of a singlet exciton to an adjacent chromophore of $\tau_{min} \sim 1$ ps, comparable to the value for the ladder-type poly-phenylene. The value of σ is consistent with the variance of the high energy wing of the fluorescence band which is $\sim 0.5\ \sigma$. By considering the Stokes shift between the 0-0 origins of absorption and emission, the electronic origin of the $S_1 \rightarrow S_0$ transition is predicted to be 2.53 ± 0.05 eV.

Spectral diffusion must also occur in a PhPPV film doped with TNF but the effect must be gradually diminished upon increasing concentration because the lifetime of singlet excitation on the host polymer is shortened. In fig. 12, the $S_1 \rightarrow S_0$ 0-0 emission maxima determined from cw-spectra have been included on the premise that the delay time at which the spectra have been recorded is identified as the 1/e decay time of the emission (see Figure 21A). The agreement between those data sets is striking and confirms that the hypsochromic of cw-fluorescence spectra of doped systems as function of the concentration is entirely due to the decrease of the efficiency of spectral diffusion rather

than to a change of the absorption spectrum of host chromophores in the vicinity of the guest molecule.

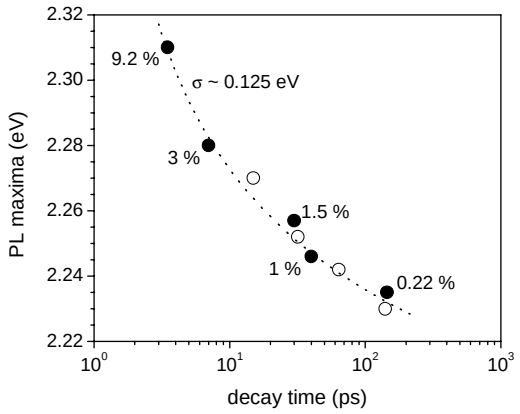

Figure 25 Maxima of the S1→S0 0-0 spectra recorded at variable delay time after excitation (open circles). The full circles indicate the peak maxima determined from cw-emission spectra upon doping with a variable concentration of TNF. They have been converted into a time dependent spectral relaxation pattern by assuming that the average emission occurs at a delay time given by the 1/e decay time. The dashed curve results from a calculation according to Mavaghar et al.[60] assuming σ = 0.125 eV.

3 Charge carrier photogeneration

In this chapter, charge carrier photogeneration behaviors were discussed mainly in form of quantum yields measured by steady state photoconduction experiments using thin films of phenyl substituted polyphenylenevinylene (PhPPV) with and without a doping of trinitrofluorenone (TNF) in a LED sandwich sturcture. The reason why these blend systems were investigated was not only to estimate typical characteristics in this material class but also to clarify whether the doping of TNF facilitates charge carrier photogeneration or not. Subsequently, detail TNF concentration dependant experiments were carried out to estimate quantitative effects of TNF doping, which is systematically added. By performing these tests, one can verify the molecular dissociation formalism as an explanation for underlying charge carrier photogeneration mechanism. Finally, one can answer the puzzle why photogeneration in PPV-derivatives can take place within $S_1 \leftarrow S_0$ 0-0 transition range, whose absorbed photon energy is not enough to dissociate directly in a molecular picture. Results of this chapter were publicated in J. Chem. Phys., 2002. (see publication list on page 4).

3.1 Experiment

3.1.1 Preparation

Homogenous films with thickness of about 100 nm were deposited on either semitransparent aluminium or indium tin oxide (ITO) covered glass substrates by spin coating from 0.7 (or 0.5) wt.-% toluene solutions. The film thickness was measured by a Dektak surface profileometer. The semi-transparent Al contacts had a typical thickness of 10 nm and were evaporated onto glass substrates in a vacuum chamber at < 10^{-5} mbar. After spin coating, Al top contacts of 7 mm^2 active area were evaporated on the polymer films. Prior to top electrode evaporating the films were kept in the vacuum chamber at room temperature for at least 12 h in order to remove volatile impurities, e.g. residual solvents. Doped polymer films were spin coated, for instance, from a 0.7 wt.-% PhPPV / 0.01 wt.-% TNF solution in toluene. Typical sample geometry and the relevant energy levels are illustrated in Figure 26 and Figure 27, respectively.

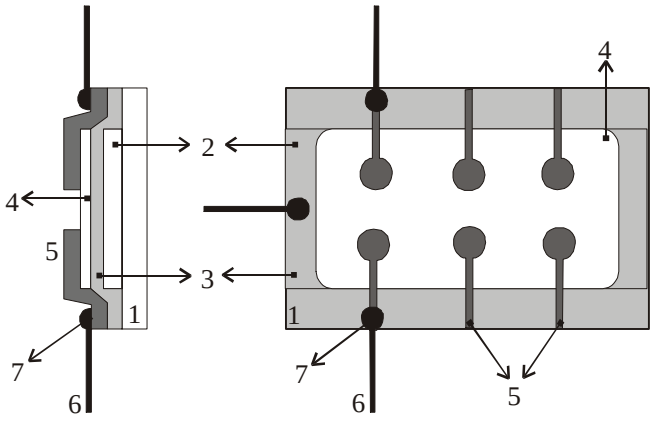

Figure 26 Schematic device structure, 1. glass substrate, 2. ITO, 3. active layer, 4. dye layer, 5. Al electrodes, 6. conneting wire, 7. graphite contact

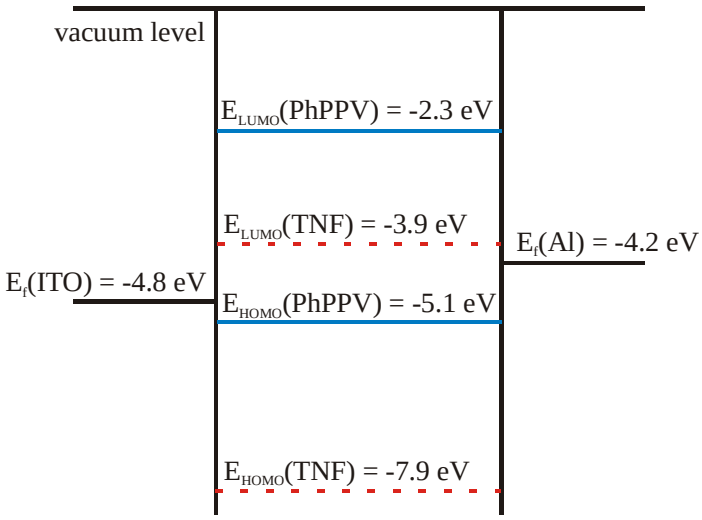

Figure 27 Scheme of the relevant energy levels.

3.1.2 Measurement

Photocurrent measurements (Figure 28) were performed in a temperature-controlled cryostat with a combination of monochromator and a xenon lamp as a light source. Photocurrent signals were detected with a lock-in amplifier (Stanford Research Systems, Model SR 850 DSP), which was connected to a chopper with a chopping rate of either 20 Hz or 400 Hz positioned between the cryostat and the light source. The benefit of the lock-in technique is that it automatically subtracts the dark current from the measured signal. In order to check the stability of the photocurrent signal time-resolved photocurrent traces within the time interval up to 30 - 60 s were recorded. It turned out that at repetition rate of 20 Hz the photocurrent war strictly constant whereas at 400 Hz some decay was noted. This is an indication that a dark periode of 50 ms is sufficient to get rid of any space charge, mostly electrons, which might have been trapped during within 50 ms exposure. Nevertheless the samples were shortened and kept in the dark

for at least several minutes after every dozen of measurements to eliminate any possible space-charge effects. To calculate the electrical field in ITO/PhPPV/Al diodes a built in potential of 0.6 V between Al and ITO electrodes has been taken into account.

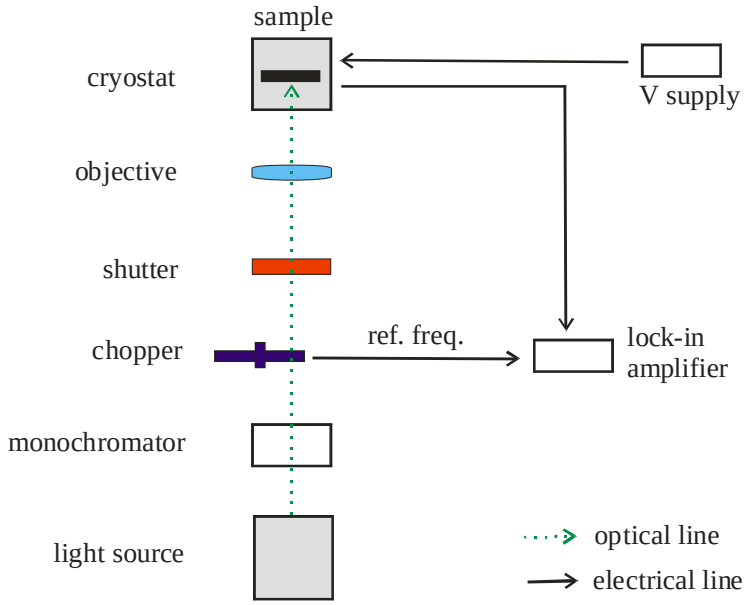

Figure 28 Scheme of steady state photocurrent measurements.

3.1.3 Charge carrier photogeneration quantum yield calculation

The quantum yield was calculated from the measured photocurrents taking into account corrections for the light source performance and the light absorption in the glass substrates, contacts, and in the active areas of the films. Spectral dependencies of the corresponding optical densities were measured with Perkin-Elmer, Lambda 9 UV/VIS/NIR Spectro-photometer.

The definition of charge carrier photogeneration quantum yield is a fraction of generated charge carrier number (N_{ch}) per absorbed photon number ($N_{abs.ph}$),

$$\varphi_{ph} = \frac{N_{ch}}{N_{abs.ph}}. \qquad (6)$$

In the praxis, a generated charge carrier number can be calculated from a measured photocurrent, $I_{ph} = N_{ch} \cdot e$. An absorbed photon number is calculated from a lamp performance and a fraction of active material absorption.

$$N_{abs.ph} = n(all\ \ photons\ \ from\ a\ lamp) \cdot n_{abs} = \frac{P_{lamp}}{h\nu} \cdot n_{abs} \qquad (7)$$

As a result, one can obtain the following equation to calculate a quantum yield for a common steady state photoconduction measurement.

$$\varphi_{ph} = \frac{I_{ph}}{P_{lamp} \cdot N_{abs.ph} \cdot e} = \frac{I_{ph} \cdot h\nu}{P_{lamp} \cdot n_{abs} \cdot e} \qquad (8)$$

To estimate a fraction of active material absorption in a device, one should be careful due to its complexities, reflections at every interface, scattering and absorption in each medium, and also wave guiding effect as illustrated in the Figure 29. Here, an example to take into account the reflection (I_3) from the last electrode (Al2) into the active layer, which is sandwiched between semi transparent Al electrodes (Al1 and Al2).

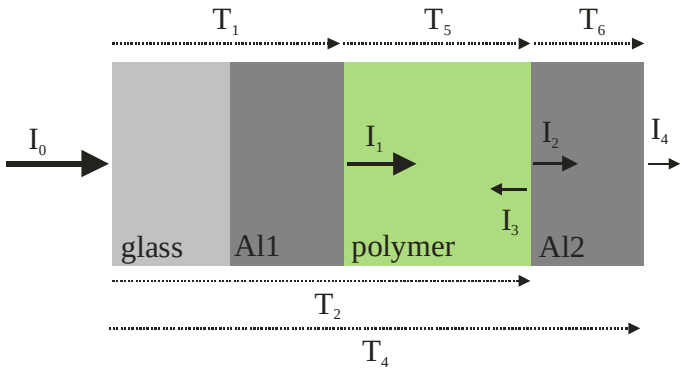

Figure 29 Absorption of active layer in a LED device.

As usual, transmittances T_1, T_2, T_4 can be directly and separately measured, then the rest transmittances can be also calculated from the measured values according to the following relations.

$$T_1 \times T_5 \times T_6 = T_4, \quad T_1 \times T_5 = T_2, \quad T_2 \times T_6 = T_4 \qquad (9)$$

After these, the reflection at the last electrode (Al2 in the above figure) can be calculated with following equations and a reflection coefficient at Al of 80 %.

$$T_2 = I_2 / I_0 = (I_2 \times 0.8) / I_0 \qquad (10)$$

In order to calculate the exact quantum yield, one should decide whether the generation type is intrinsic volume ionization in the full active area or extrinsic surface sensitized charge carrier photogeneration. If the type of charge carrier photogeneration is assumed as an intrinsic case, the quantum yield can be calculated by dividing the number of generated electrons by the full number of absorbed photons in the active film.

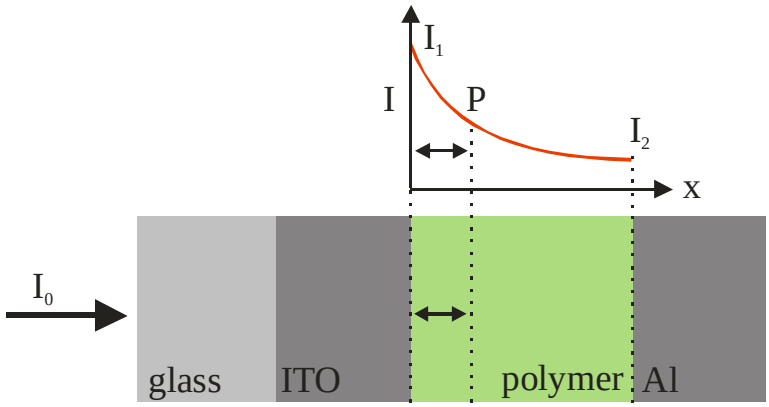

Figure 30 Diagram for surface correction.

But if the charge carrier photogeneration is mainly an ITO surface sensitized case, the electrode-sensitized current has to be normalized to the number of the photons absorbed within a thin layer of thickness l_d from the ITO/film interface, i.e. to $I_0 \cdot \alpha \cdot l_d$ where I_0 is the intensity at the interface and α = 2.3 OD / L is the penetration and OD is the optical density of a film of thickness L.

3.2 Results

The optical absorption and photoluminescence (PL) spectra of an approximately 100 nm thick PhPPV film deposited on a quartz substrate are shown in Figure 15. The absorption spectrum is unaffected by doping. In contrast, TNF doping dramatically reduces the PL intensity.

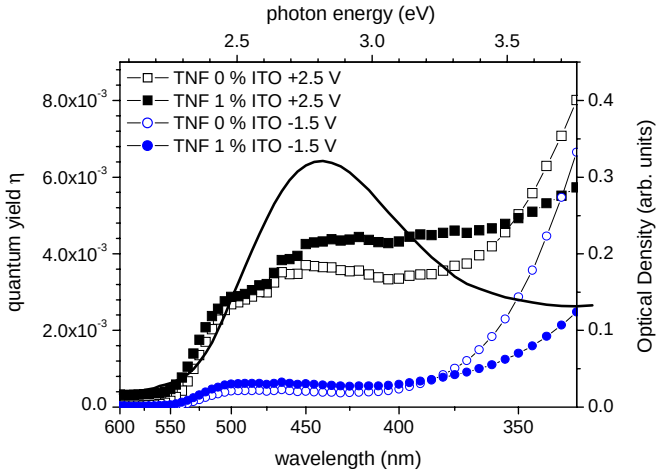

Figure 30 Spectral dependences of the charge carrier photogeneration quantum yield η in ITO/PhPPV/Al configuration at 293 K. The electric fields for both bias directions were approximately 2.5 x 10^5 V/cm.

Figure 30 compares the spectral dependences of the photocurrent upon an irradiating a neat PhPPV film and a film doped with 1 % TNF through an ITO electrode at either positive or negative bias. In both cases the current has been normalized to the number of photons absorbed within the film. Regarding the spectral range of the $S_1 \leftarrow S_0$ transition, there are several noteworthy observations. (i) At positive bias the current is roughly 5-times higher but at higher photon energies that anisotropy tends to vanish. (ii) The photocurrent yield, as defined above, depends on polarity; while at negative polarity a

weak maximum coincident with the absorption maximum is observed. (iii) Doping has no major effect, the increase is roughly by 50 % only. Upon replacing ITO by a semi-transparent Al electrode the anisotropy of the photocurrent vanishes and absolute yields are comparable to that upon shining light through the negative ITO electrode (Figure 33).

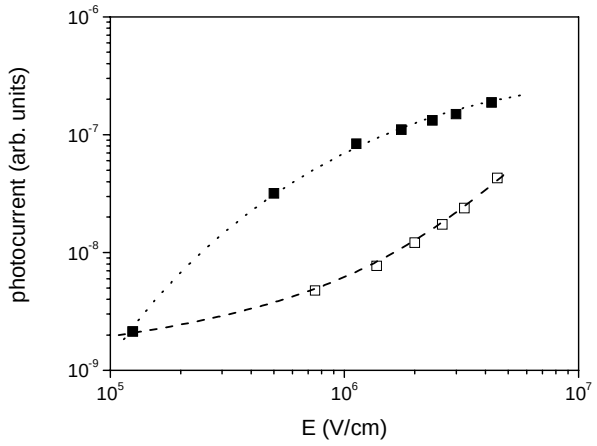

Figure 31 Field dependence of the photocurrent in ITO/PhPPV/Al configuration at 293 K using excitation wavelength of 460 nm (2.7 eV). The filled squares are for positive bias at ITO, open squares are for negative bias at ITO.

Again, 1 % TNF-doping has only a small effect. Since the field dependences of the current at positive bias at ITO and at reverse polarity or upon irradiating through Al are also different (Figure 31), it is straightforward to assign the forward-current to hole injection from an ITO-anode. Under opposite polarity charge carriers are generated in the bulk implying that no injection occurs at either positive and negative bias of Al. Using this normalization the action spectrum of electrode-sensitized current starts at the very tail of the absorption spectrum and stays constant up to $h\nu \sim 3$ eV (Figure 32). In

the doped film yield increases slightly with photon energy. It is obvious that the absolute yield must depend on the assumed thickness of the active layer.

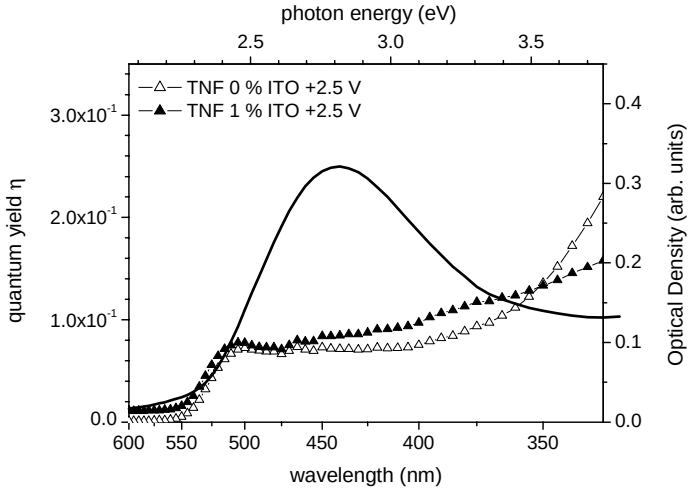

Figure 32 Quantum efficiency of the forward current in ITO^+/PhPPV/Al configuration at 293 K assuming that photogeneration occures within 5 nm thick layer next to the irradiated ITO anode. The raw data are taken from Figure 30.

Since we wanted to clarify the effect of doping the photocurrent was measured as a function of concentration of TNF Al|PhPPV|Al diodes where sensitized injection is absent. In Figure 33 shows at set of representative spectra. It shows that the concentration dependence depends on the spectral range. Within the $S_1 \leftarrow S_0$ absorption band (2.76 eV) the charge carrier photogeneration yield is almost independent of concentration up to c ~ 2 %, and increases slightly at higher concentrations. At hν = 4.13 eV the yield decreases slightly with concentration and, after passing a minimum, it increases again.(Figure 35)

A non-Arrhenius temperature dependence of the photogeneration yield with the apparent activation energy decreasing with temperature was a common feature in all samples, noting, however, that a slightly steeper *T*-dependence was observed in ITO/PhPPV/Al structures as compared with Al/PhPPV/Al diodes (Figure 35). Another general trend is that the temperature dependence becomes weaker with increasing photon energy. No hysteresis effect was observed upon cooling down to 100 K and heating up to 300 K.

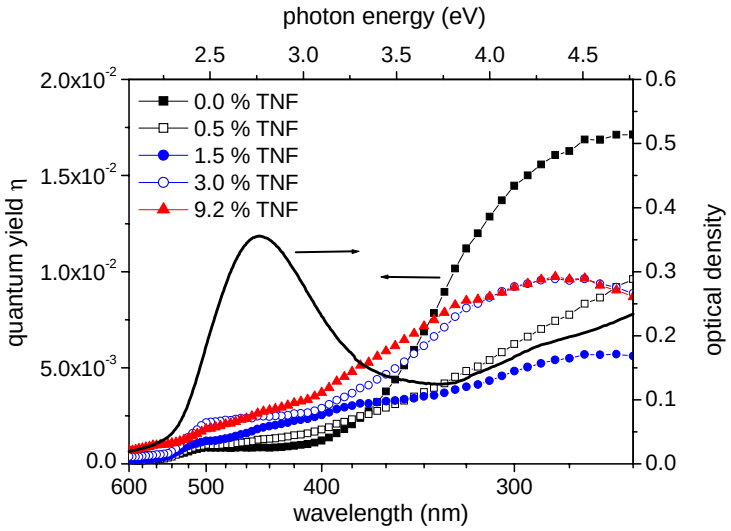

Figure 33 Action spectra of bulk photocurrents in Al/PhPPV/Al configuration at various TNF concentrations. The electric field was 2.5 x 10^5 V/cm.

Independent of photon energy, the dependence of the photoconductivity upon the incident light intensity was strictly linear (Figure 34). This indicates that bimolecular charge carrier recombination and space-charge effects are unimportant. Concomitantly, it proves that the photocurrent is a direct measure of the charge carrier generation rate.

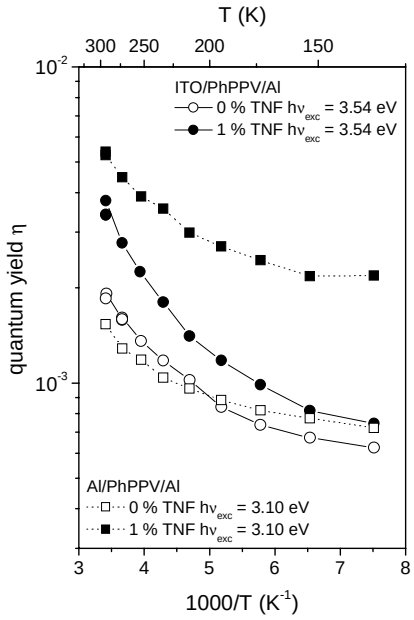

Figure 35 Temperature dependence of the carrier photogeneration quantum yield η in Al/PhPPV/Al and ITO^+/PhPPV/Al samples in the absence and presence of 1 % TNF. The electric field was 4.4 x 10^5 V/cm in the doped film (filled squares), 4.7 x 10^5 V/cm in the neat film (open squares), 2.7 x 10^5 V/cm in the doped film (filled circles) and 2.5 x 10^5 V/cm in the neat film (open circles).

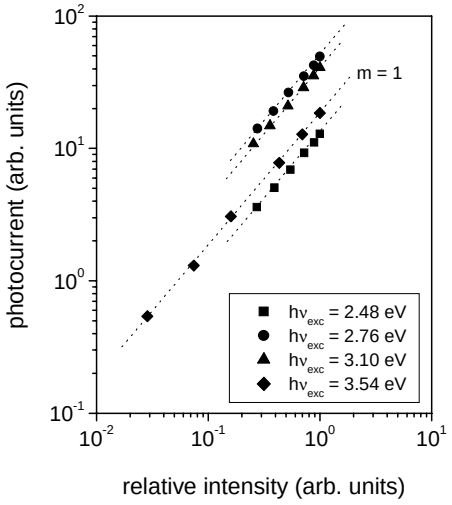

Figure 34 Intensity defendence of the carrier photogeneration quantum yield η of PhPPV at 293 K for various excitation photon energies. The electric field was 2.5 x 10^5 V/cm.

3.3 Discussion

3.3.1 Exciton induced photoinjection at the electrode

When an exciton in a molecular solid diffuses towards an electrode where empty acceptor states are available, i.e. electron states above the Fermi level of the electrode or dye molecules with low lying lowest unoccupied molecular orbitals (LUMOs), it can transfer its electron to the electode and the remaining hole can contribute to a unipolar photocurrent. The process is asymmetric regarding to the sign of the applied bias. In p-type materials exciton the anodic process prevails. Experiments on a ladder type poly-(phenylene) (MeLPPP), in which optical excitation occurred through a positively biased ITO electrode without and with a thin interfacial layer of SiO, confirmed both the existence of the effect and its prevention by a layer which blocks electron transfer towards the ITO.[29]

The absence of the effect upon reverse bias is probably due to efficient trapping of the electron next to the interface. Figure 30 confirms that at positive bias sensitized hole injection at an ITO/PhPPV interface occurs. It is remarkable, though, that the effect is almost the same for a neat sample and a sample doped by 1 % of TNF although doping decreases the life time of singlet excitations by 2 orders of magnitude. Thus exciton diffusion towards the interface cannot be the rate controlling for sensitized injecting. Instead one has to invoke rapid dissociation of the S_1 excitation into a geminatly bound e..h pair, sensitized by TNF or an inadvertant dopant, and subsequent transfer of the sibling electron to the electrode. The consideration of the injection yield as a function of

the electric field supports this notion. Assuming that at high electric field all interfacial e..h pairs contribute to the photocurrent one can estimate the thickness of the layer within which sensitized injection operates. It turns out to be 5 nm.

The sensitization effect vanishes upon both reversing the bias and replacing the ITO-anode by Al. Since metal electrons can quench singlet excitations generated close to the interface by dipole-dipole coupling this effect appears to be obvious.[65] However, in view of the above the consideration of the mechanism of sensitization at an ITO-electrode, it is more likely that it is caused by the Al_2O_3 layer at the interface which blockes transfer of the electron of the geminate pair across the interface rather than the reduction of the exciton lifetime.

3.3.2 Photogeneration near the absorption edge.

The essential question addressed in this section is whether or not photogeneration within the spectral range of the vibronic $S_1 \leftarrow S_0$ absorption band is whether or not a relaxed S_1 excitation, i.e. a S_1 excitation not coupled with a molecular vibration, is able to generate a pair of charge carriers without participation of a sensitizer. This question is open to conjecture because it is known that in conjugated polymers some fraction of singlet excitations are able to dissociate into a geminately bound e..h pair not requiring a chemically distinct sensitizer. Evidence comes delayed intrinsic fluorescence from a ladder-type poly-(phenylene) due to the recombination of geminate e..h pairs,[66] noting, however, that in those experiments bimolecular annihilation of singlet excitations occurred. The process is sensitive to an external electric field and requires

that in average the energy of a coulombically bound e..h pair must be only slightly above the S_1 energy. Disorder effects tend to diminish that energy difference. Theoretical calculations support this reasoning[67] as do the observation of thermally stimulated photoluminescence at low temperatures.[68] The qualitative explanation why in this respect conjugated polymers differ from classic molecular solids is that the S_1 excitation is more extended than for instance in a molecule of the acene family (e.g. anthracene) and, concomitantly, the transfer of a charge across a neared interchain distance requires very little energy only implying the exciton binding energy E_b is mostly due to the coulombic binding energy of the pair. However, an E_b of the order of 0.5 eV should give rise to activated behaviour with an activation energy comparable to E_b. This is at variance with experiment.

In general, the measured temperature dependences of photogeneration within the spectral regime of the $S_1 \leftarrow S_0$ transition band are non-Arrhenius-like. At low temperatures the yield tends to approach a constant value. In fact, e..h dissociation in an energytically random hopping system must be feature for such a temperature dependence. The reason is related to energetic relaxation. If a charge carrier generated with the center of the density of states distribution (DOS) of Gaussian shape, it will relax towards the tail states in the course in hopping inside the coulombic well. This process becomes the more important the lower the temperature is and the energy gained by relaxation can partly and, in the extreme case, fully compensates for the activation energy needed to overcome the coulombic barrier.[69] However in the high temperature limit $\varphi(T)$ should extrapolate to an Arrhenius law with an activation energy identical to the average coulombic binding energy of the e..h pair. Obviously, the experimentally

observed φ(T) dependence is qualitatively recovered by theory but the absolute value of the activation energy is some 20 % of the anticipated exciton binding energy only. One way to solve this puzzle is to invoke extrinsic effects, i.e. sensitization by either inadvertent or intentionally added. By investigating the effect of controlled doping one can extrapolate to the behavior of neat samples.

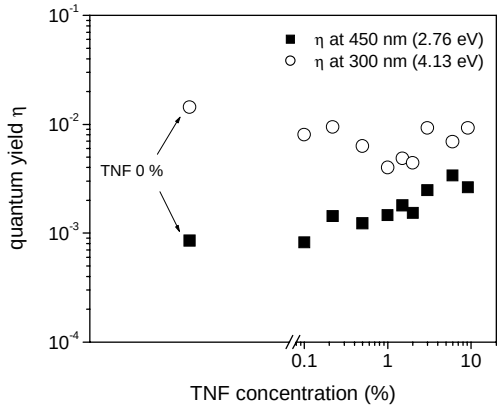

Figure 35 Quantum yield of photogeneration at 293 K as a function of the TNF concentration, probed at h ν_{exc} = 2.76 eV and 4.13 eV.

The Figure 35 shows that by adding TNF at a concentration between 0.1 and ca. 9 wt.-% the photocurrent does increase but highly sub-linearly only. The simultaneous measurement of the fluorescence quenching provides a straightforward explanation of this phenomenon.[64] The operationally the simplest way to quantify the effect of doping is to analyse the reduction of the fluorescence decay time as a function of concentration after pulsed excitation. The rate equation for the concentration of singlet excitation is

$$\frac{d[S]}{dt} = -[k_r + k_{nr} + k_{q.0} + k_q c]\cdot[S], \qquad (11)$$

where k_r and k_{nr} are the rate constants of intrinsic radiative and non-radiative decay, $k_{q.0}$ and $k_q c$ are the rate constants for quenching by unidentified quenchers and deliberately added dopants at concentration c, and $[k_{q.0} + k_q c]\cdot[S]$ the rate of singlet quenching. From the experimentally determined fluorescence lifetime τ of a PhPPV as a function of concentration shown in ref. 64, it is known that τ does not extrapolate to the intrinsic lifetime τ_0 at zero concentration of TNF. Instead, there is a residual quenching effect at c = 0 due to an unidentified quencher present at a concentration of ≤ 0.04 %.

Provided that the light intensity is below a critical level beyond at which non-linear terms in the rate equation become important, e.g. exciton-exciton annihilation, the relevant terms in the rate equation for cw-excitation are the same. Under this premise the relation quenching events can be inferred from the relative loss of fluorescence,

$$Q = \frac{I_0 - I(c)}{I_0} = \frac{k_{q0} + k_q(c)}{\sum_i k_i}. \qquad (12)$$

Provided that the number of quenching events is proportional to the photogeneration yield, concentration dependence of both the yield and quenching should be proportional. If k_{q0} = 0, Q should decrease linearly with decreasing concentration of the dopant. However, if about 50 % of the singlets are already quenched by accidental doping the total defect sensitized photogeneration can increase by a factor of 2 only at complete singlet quenching. Considering the uncertainly regarding absolute photogeneration yields this effect can hardly be distinguished. This is the reason why the photogeneration yield is almost constant even at low dopant concentration.

The yield of complete dissociation of a strongly coulombically bound e..h pair is much less than unity and strongly depends on external electric field. However, its temperature dependence is weak without noticeable spectral dependence except at large doping. The fact that (i) in the undoped sample the photogeneration yield is closed to that of a sample of c < 0.1 % and (ii) the concentration of inadvertent dopant, which cause fluorescence quenching [64] in the neat material, is comparable suggests that both effects have the same origin, i.e. that the photocurrent in the spectral range of the $S_1 \leftarrow S_0$ transition is defect sensitized. It is still an open question whether the defect are chemical or physical origin. The latter type of defect could be a pair of chains which are tightly bound so that e..h pair is more strongly bound than a S_1 excitation. The present experiments do not allow differentiating between the two possibilities.

It is obvious that doping a conjugated polymer by a dopant with lower/higher lying LUMO/HOMO gives rise to radical anion and cation states as precursors for photoconduction. The still open question is how the coulombic energy can be overcome, in particular since the dissociation yield is << 1 yet only weakly temperature dependent. One conceptual possibility is that the release of energy following electron transferring from the excited donor to the acceptor assists further dissociation of the geminately bound e..h pair. If so, the energy levels of the dopants have a major effect on the efficiency because it determines the excess energy. Dissociation of a relaxed S_1 state at a physical dimer should be much less efficient than that at a PhPPV:TNF pair where the LUMO levels of host and guest differ by about 1.6 eV.

The polarity independent increase of photogeneration of higher photon energies has been explained in terms of the model for dissociation of vibrational hot excitons. The action spectrum of intrinsic photogeneration in undoped PhPPV (Figure 33) is no different from that of other conjugated polymers and features an onset at 3 eV. It is remarkable, though, that at zero-order approximation, the magnitude of the yield and its spectral dependencies is basically retained upon doping by TNF (see Figure 33). Since doping decreases the lifetime of S_1 exciton, this is unambigious proof that the intrinsic contribution to photogeneration at higher hν cannot be due to "cold" S_1 excitation. Instead, it must either be due to autoionization from the primarily excited Franck Condon state[70] or dissociation of electronically "cold" S_1 excitation, or, rather coulombically strongly bound e..h pairs couple to a temporally hot vibrational heat bath.[14, 71]

However, there are subtle differences. Plotting the photogeneration yield at hν = 4.13 eV as a function of concentration shows that φ drops by a factor of 3 upon increasing the TNF concentration features a shallow minimum and increases again for $c \geq 2$ %. Such a behavior is at variance with the ballistic dissociation[70] concept because the lifetime of the initially excited Franck Condon state must be unaffected by its future decay. The concept of hot exciton dissociation provides a plausible explanation, though. If the exciton is excited next to a TNF molecule it can transfer its electron on a time scale of ≤ 1 ps. Since donor and acceptor from quantum mechanically coupled system part of the excess energy will be transferred to the TNF. Therefore the lifetime of the excess vibrational bath decreases and, concomitantly, the dissociation yield will decrease. At the same time the action spectrum of that process changes because of

electron trapping at TNF is an exothermic process. At lower photon energies, when in the absence of doping the excess thermal energy is insufficient to promote on-chain dissociation, part of the reaction energy can be used to accomplish e..h dissociation. Therefore the process starts at lower excess photon energies already. By the way, this spectral change upon doping is another proof against any correlation with optical absorption spectrum and against identifying the photoelectronic threshold with the exciton binding energy. The fact that the relative increase of the dissociation yield at higher concentrations is independent of photon energies suggests that it is related to charge transport. At high TNF-loading the electron at the TNF is no longer immobile but can execute a percolative motion. This should be decrease the yield of geminate TNF^-:$PhPPV^+$ pairs.

4 Charge Carrier Mobility

In this chapter, charge carrier mobility of poly phenylenevinylene-ether (PPV-ether) were estimated using two types of time-of-flight techniques, a conventional bulk excitation and a surface sensitized injection using rhodamine 6G (R6G) as a charge carrier generation layer. Using the time-of-flight method, mobilities of holes or electrons can be estimated relatively independent of external effects, for instance, complicated injection behaviors from electrodes and also bimolecular e..h recombinations using a proper choice of experimental conditions and device structures. Mobility values at room temperature are crucial and also enough to compare qualities of π-conjugated polymers as an active material in optoelectronical devices. Such devices are usually used at room temperature. However, an extended investigation over a wide temperature range is of importance to verify the hopping transport model in a precise physical manner, furthermore, to distinguish it from the polaron transport model. Such a detailed study can also give more insight information into disorder effects during charge carrier hopping transport processes within a Gaussian type density of states (DOS), in which site energies are randomly distributed. Results of this chapter were also publicated in J. Chem. Phys., 2000. (see publication list on page 4)

4.1 Measurement

A photoluminescence yield of 82 % in solution testifies on the absence of nonradiative quenching centers, such as oxidation products, in the polymer chain. The absorption and fluorescence spectra of a 100 nm thick film are shown in Figure 36.

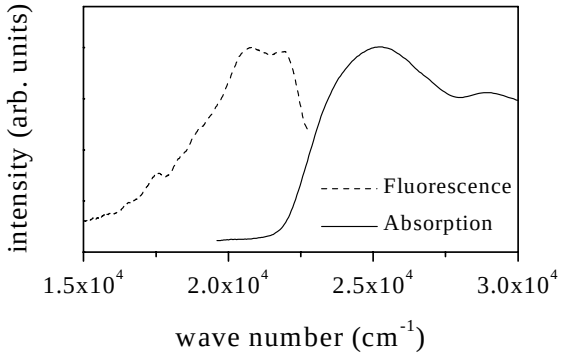

Figure 36 Absorption and fluorescence spectra of PPV-ether by 295 K.

Films with thickness of 2.2 μm were prepared via the Doctor Blade technique while a 5.4 μm thick film was cast from solution. Before evaporating a typically 150 nm thick aluminum top contact, the samples were stored for 12 h under reduced pressure of 10^{-6} mbar. The active area of the devices was 7 mm^2. Film thicknesses were measured by a Dektak surface profiler. Single shot transient photocurrents were recorded with the time of flight (TOF) technique (see Figure 37 for the experimental setup and Figure 38 for the used circuit configuration), using either bulk photogeneration or charge injection from a rhodamine 6G generation layer. The latter was vapor deposited on top of the PPV-ether film prior to the deposition of the Al-electrode and had a thickness of 10 ~ 12 nm. Photoexcitaton occurred through the ITO-side of the device using an optical

parametric oscillator (OPO) which delivered 10 ns pulses of 3.13 eV and 2.23 eV photons. The photon dose was adjusted on the premise that the total charge was less than 5 % of the capacitor charge. From the bias dependence of the TOF-signals it was clear, that holes were the majority carriers.

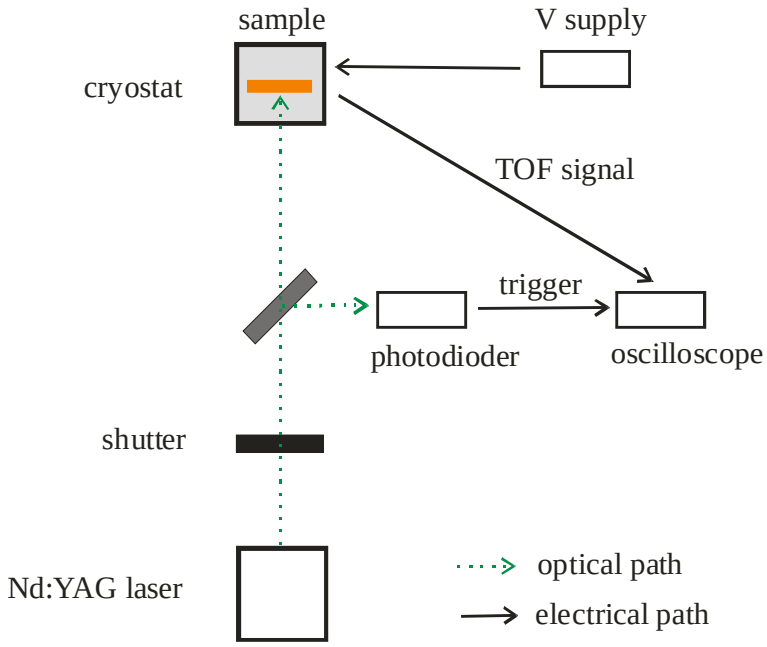

Figure 37 A scheme of time-of-flight experimental setup.

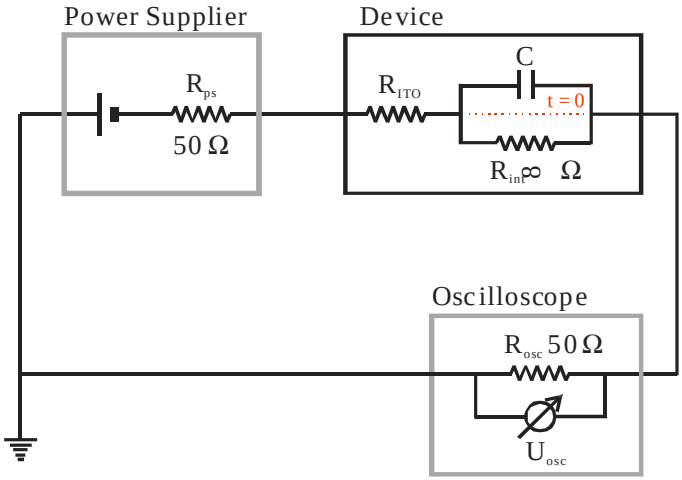

Figure 38 A circuit scheme of TOF experiment.

4.2 Results

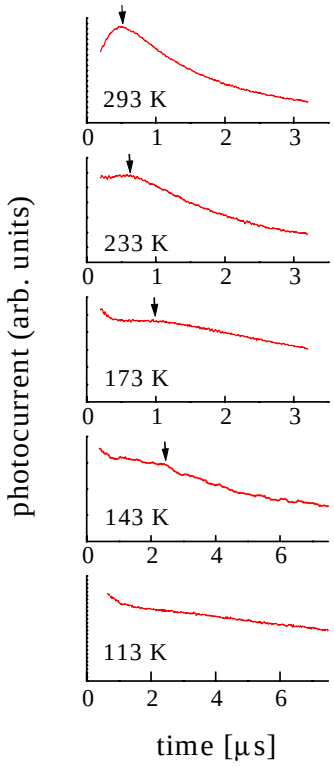

Figure 39 TOF signals in PPV-ether at different temperatures and at a field of 9.5 x 10^5 V/cm. The samples were excited into the $S_1 \leftarrow S_0$ transition (hν = 3.13 eV). The sample thickness was 5.4 μm.

Time of flight signals recorded with a 5.4 μm thick PPV-ether film upon photoexcitation at 3.13 eV, i.e. within the range of the $S_1 \leftarrow S_0$ absorption band are presented in Figure 39. After a fast, initial decay the current settles to a plateau and decays smoothly afterwards. At higher temperatures a cusp develops independent of the number of transported charges. The plateau-character of the signal is preserved to temperatures as low as 140 K. At lower temperatures the signals become dispersive. The hole mobility has been inferred from the time at which the tangents to the TOF signal intersect although it is recognized that by this procedure one keeps track of the fastest

carriers only. However, the functional dependences are independent of data analysis[72]. Their variance W, defined by

$$W = \frac{t_{1/2} - t_0}{t_0} \qquad (13)$$

where $t_{1/2}$ is the time after which the current has decayed to one half of the plateau value, is typically 0.7. The shape of the TOF signals is almost independent of the electric field except that at higher fields a weak cusp appears.

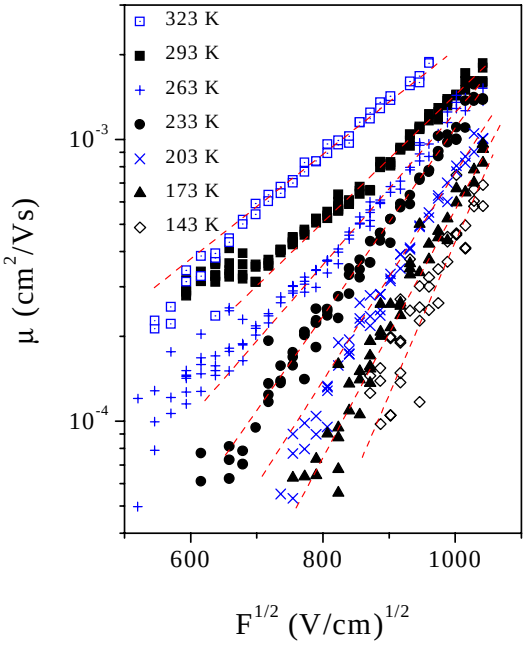

Figure 40 Field dependence of the hole mobility parametric in temperature upon intrinsic excitation

The field dependence of the hole mobility features a $\ln \mu \propto F^{1/2}$ law. The slope $S = \partial \ln(\mu/\mu_0) / \partial F^{1/2}$ increases with decreasing temperature (Figure 40). The temperature dependence of μ is plotted in Figure 41, both on an Arrhenius scale and on a $\ln \mu$ vs. T^{-2} scale. Zero field values have been calculated on the premise that the $\ln \mu \propto F^{1/2}$-law

extends to $F \rightarrow 0$. Extrapolating $\ln \mu \propto T^{-2}$ to higher temperatures yields $\mu(T \rightarrow \infty) \cong 3 \times 10^{-3}$ cm^2/Vs while Arrhenius plots give 2 - 3 times larger values.

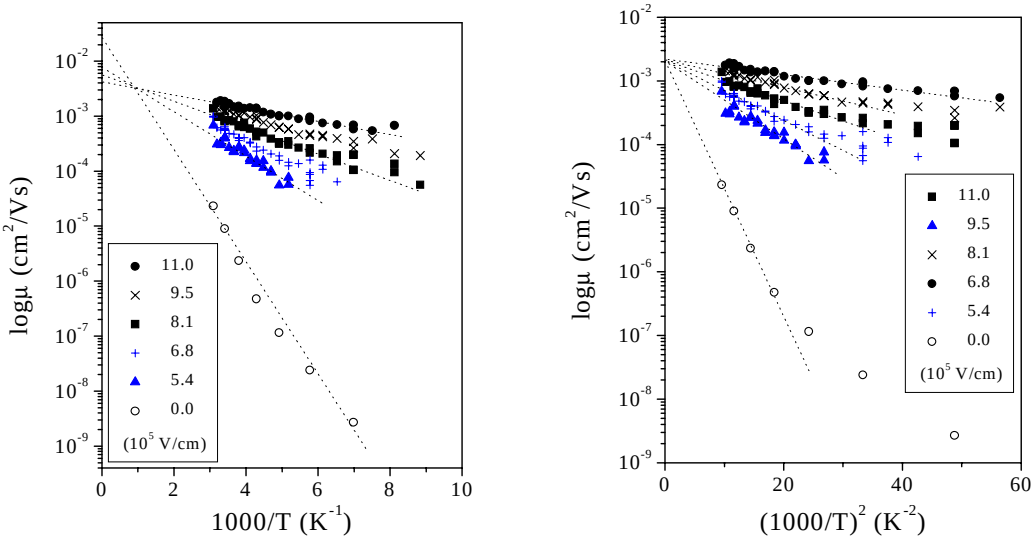

(a) (b)

Figure 41 Temperature dependence of the hole mobility parametric in electric field plotted on an ln μ vs T^{-1} scale (a) and on a ln μ vs. T^{-2} scale (b), respectively.

The pattern of TOF signals is changed upon photoinjection from a thin rhodamine 6G layer between the PPV-ether film and the Al anode. The behavior is very much like that in low molecular glasses or molecularly doped polymers upon injection from a generation layer.

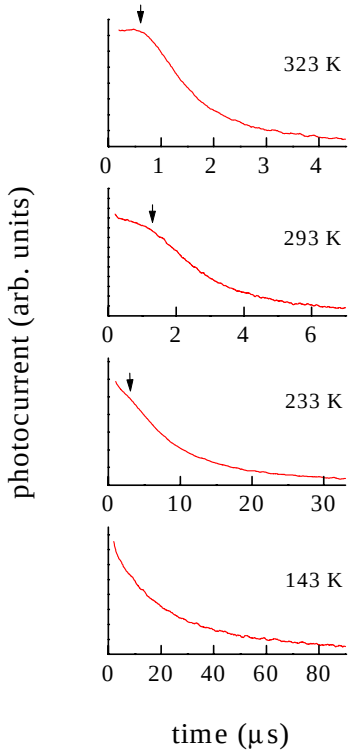

Figure 42 TOF-signals at different temperatures and an electric field of 4.1 x 10^5 V/cm upon photoinjection from a rhodamine 6G layer excited at 2.23 eV. The sample thickness was 2.2 µm.

It is remarkably, though, that for comparable temperatures the intersection point in TOF signals upon intrinsic and extrinsic photogeneration and displayed on double logarithmic scales agrees within a factor of 2 with the time at which the arrival signal is detected upon bulk excitation but displayed on linear scales, taking into account of the field dependence of µ (see Figure 40). Both the cusp, seen in high temperature TOF-signals upon intrinsic excitation, is lost and the dispersion commences for T ≤ 200 K (Figure 42)

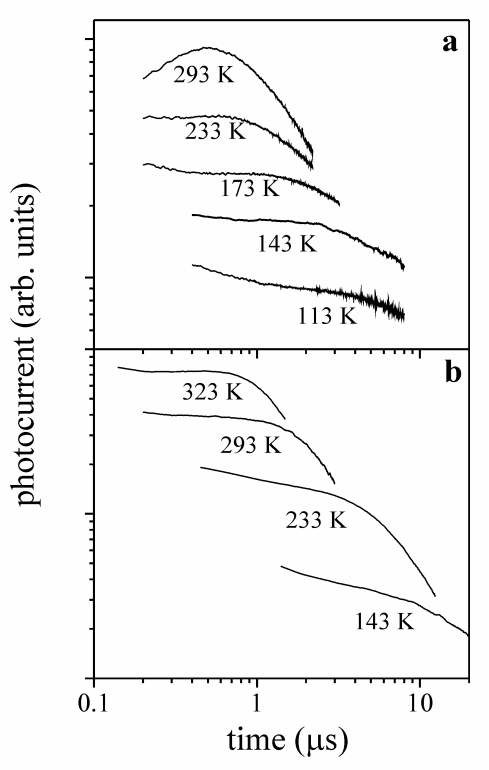

Figure 43 Double logarithmic representation of the TOF signals. a) Data are taken from Figure 39 (intrinsic excitation) and b) Figure 42 (extrinsic excitation).

4.3 Discussion

The fact that the temperature dependence of the hole mobility in PPV-ether at different electric field features straight lines if plotted on an Arrhenius scale, intersecting at an effective temperature ($T^* \cong 1200$ K) might suggest the applicability of Gill's[73] phenomenological data analysis, i.e

$$\mu(T,F) = \mu_0 \exp\left[-(\Delta - \beta F^{1/2})/kT_{eff}\right], \qquad T_{eff}^{-1} = T^{-1} - T_0^{-1} \qquad (14)$$

It rests upon the notion that charge transport is controlled by traps which are changed when empty yielding a Poole-Frenkel-type field dependence, i.e. $\beta = (e / \pi \varepsilon \varepsilon_0)^{1/2}$,

where ε is the dielectric constant. For ε = 3.5, β = 4 x 10^{-4} $(Vcm)^{1/2}$ is predicted. However, when plotting the effective activation energy $\Delta^{eff} = \Delta - \beta F^{1/2}$ determined from Figure 41a versus $F^{1/2}$ (Figure 44) yields a value which is by one order of magnitude lower, i.e. β = 4 x 10^{-5} $(Vcm)^{1/2}$.

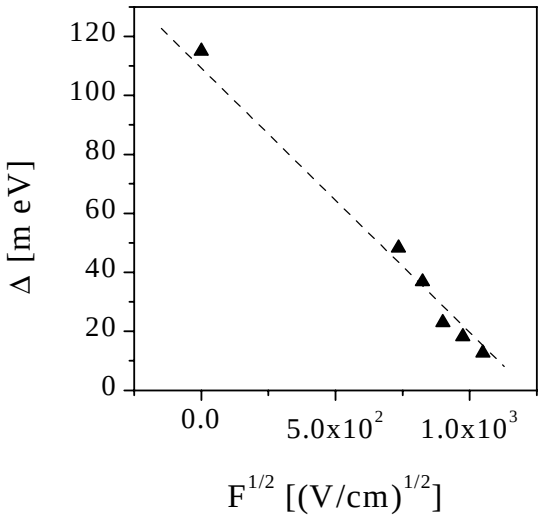

Figure 44 Field dependence of the apparent activation energy of the hole mobility inferred from the Arrhenius plots (Figure 41a).

Apart from the general problem that the assumption of charged traps is unjustified, lowering of a coulombic energy barrier by the electric field cannot be responsible for the μ(F)-dependence. On the other hand, inhomogeneous broadening of absorption and fluorescence spectra of PPV-ether (Figure 36) prove unambiguously that disorder must be important. It can be characterized by an inherent, broad distribution of localized states among which both charge and exciton transport occurs. As far as charge transport is concerned, this must give rise to (i) a temperature dependent activation energy of charge carrier hopping, (ii) a field dependent mobility of the form ln $\mu \propto F^{1/2}$, (iii)

anomalously broad tails of TOF-signals, and (iv) the occurrence of dispersion below a critical temperature. The functional dependence should be characteristic for the type of the density of states distribution (DOS). Previous Monte Carlo simulations for hopping transport within a Gaussian DOS predicted[74]

$$\mu(T,F) = \mu_0 \exp\left[-\frac{2}{3}\hat{\sigma}^2\right]\exp\left[-C(\hat{\sigma}^2 - \Sigma^2)F^{1/2}\right] \qquad (15)$$

where $\hat{\sigma} = \sigma / kT$, σ is the variance of the DOS, Σ is a measure of off-diagonal disorder and C is an empirical constant, C = 2.9 x 10^{-4} $(cm/V)^{1/2}$. Meanwhile the formalism has been extended by including inter-site correlation but the gist of the argument is retained[75, 76]. The ln μ ∝ T^{-2}-type temperature dependence is due to the displacement of the center of the occupational DOS relative to the center of the DOS itself as carriers occupy deeper states upon lowering the temperature. Dispersive transport occurs where the time required for a carrier to settle to quasi-equilibrium exceeds their transit time. It depends on the thickness of the sample. For a 5.4 μm thick sample, dispersion occurs for a critical energetic disorder parameter $\hat{\sigma}_c$ = 5.2.

Formally one can cast the field dependence of the hopping motion described by eq. (15) into an effective field dependent width σ^{eff} of the DOS, i.e.

$$\mu(T,F) = \mu_0 \exp\left[-\left(\frac{2\sigma^{eff}}{3kT}\right)^2\right] \qquad (16)$$

Figure 41b. shows that above about 200 K experimental μ(T, F) data do obey eq. (16) and extrapolate to an ordinate intercept of μ_0 = 3 x 10^{-3} cm^2/Vs for T → ∞. For < 200 K ln μ vs. T^{-2} curves tend to level off. The σ^{eff} decreases with increasing electric field. It is instructive to compare related data for a molecularly doped polymer, for instance, a hole

transporting, derivative of an enamine (ENA-A) incorporated into polystyrene[37, 77] normalized to the zero field value (Figure 45). The pertinent μ(T, F)-data are in accordance with the disorder formalism for hopping motion in a Gaussian DOS. From the F → 0 intercepts of μ(T)-curves a variance of the DOS of 0.082 eV was derived.

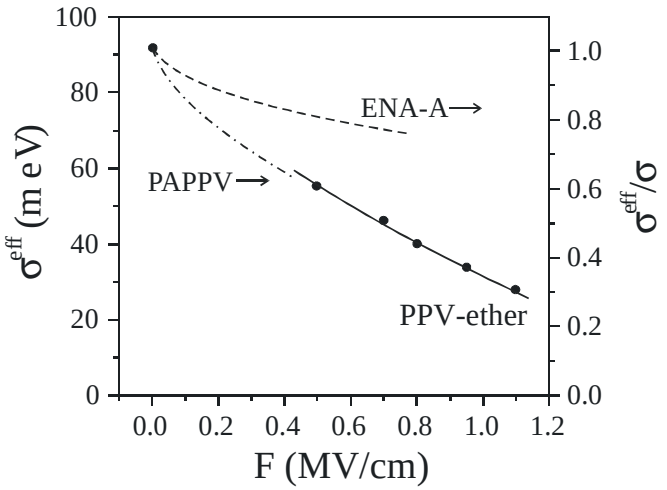

Figure 45 Right ordinate : Dependence of the effective variance σ^{eff} of the density distribution of hole transporting states as a function of the applied electric field, normalized to the few field value. Dotted and dash-dotted curves refer to a hole transport in polystyrene doped enamine(ref. 76) and a phenylamine substituted derivative of PPV (PAPPV) (ref. 41), respectively. The left ordinate refers to the absolute values for σ^{eff} in PPV-ether.

It is obvious that for PPV-ether, $\sigma^{eff}(F)$ decreases faster with increasing field. However, upon rescaling the electric field by a factor of 0.35 the ENA-A:PS data bridge the gap between the $\sigma^{eff}(F)$ for PPV-ether in the field range $0 < F < 4.5 \times 10^5$ V/cm. The straightforward explanation for this observation is that the scaling quantity is the drop of the electrostatic potential between sites relative to the width of the disorder potential rather than the electric field. Since in a conjugated polymer the charge distribution

associated with a radical cation is more extended than in a small molecule or oligomer the step length per inter-site hop has to be larger. Therefore the above scaling factor translates into a three times larger site extention as compared to the ENA-A molecule or any other transport molecule in a low molecular glass or molecularly doped polymer. Support for this interpretation comes from data for the hole mobility in a derivate of a phenylamino-substituted poly(phenylenevinylene) (PAPPV) [41]. It turns out that an analysis of μ(F) at different temperatures yields virtually the same dependence of the width of the effective DOS on the electric field as PPV-ether does. Obviously, the steeper field dependence is a signature of extended π-delocalization in conjugated polymers.

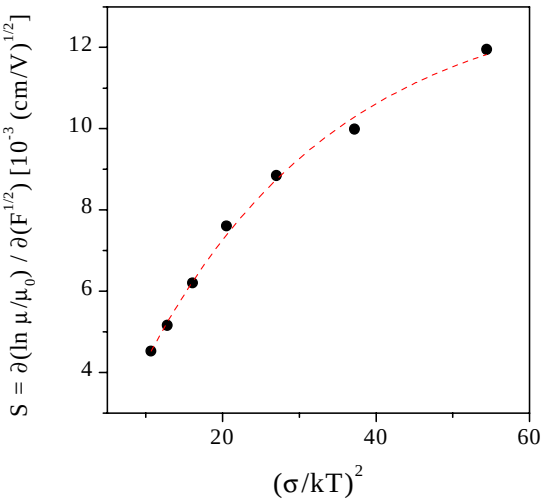

Figure 46 $S = \partial \ln(\mu/\mu_0) / \partial F^{1/2}$ as a function of $(\sigma/kT)^2$ (σ = 91 meV).

The ln μ vs $F^{1/2}$-type field dependence of the mobility is a signature of hopping within an energetically disordered DOS rather than of polaron motion. In Figure 46 the slope parameters $S = \partial\ln(\mu/\mu_0) / \partial F^{1/2}$, are plotted versus $\hat{\sigma}^2$. From eq. (15) one would expect

that S = $C(\hat{\sigma}^2 - \Sigma^2)$, i.e. $\partial S / \partial \hat{\sigma}^2 = C$ where the simulation value is C = 2.9 x 10^{-4} $(cm/V)^{1/2}$. For $\hat{\sigma}$ < 5, the data approach a straight line with C = 2.7 x 10^{-4} $(cm/V)^{1/2}$ but the absolute values of S are larger than predicted. Obviously, the concept of superposed uncorrelated energetic and spatial disorder in a system in which the sites are extended is a serious oversimplification. By the way, at lower temperatures the $S(\hat{\sigma}^2)$-dependence has to deviate from straight line behavior when the system is no longer in quasi-equilibrium.

Applying the previous criterion to the transition from non-dispersive to dispersive transport, i.e. $\hat{\sigma}_c$ = 5.2 for a sample of several μm thickness, one can predict at which temperature the transition should occur. For σ = 91 meV the critical temperature is 203 K. This is indeed in agreement with TOF experiment employing sensitized injection yet not upon intrinsic photoexcitation. In conjunction with the occurrence of a cusp in TOF signals of higher temperatures this provides additional support for the concept of hopping within an intrinsic DOS and confirms that disorder rather than polaron effects is the main source of the temperature dependence of the mobility. This does not imply that there is no structural change at all upon ionizing a hopping site, it simply means that the structural relaxation energy is sufficiently small in order not to contribute to the temperature dependence of the redox process among the sites. In the literature of TOF studies the occurance of a cusp is erratic. In some cases it has been observed in others it is absent[78, 79]. Some time ago Borsenberger et. al [80]. advanced an explanation based upon the idea that the distinguishing property is the initial occupancy of charge carriers created in a DOS of localized states. If carriers are initially generated at random

within an intrinsic Gaussian DOS they will relax to the tail states, the occupational DOS being displaced by an energy $\varepsilon_\infty = -\sigma^2/kT$ below the center of the DOS. In a TOF-experiment this gives rise to a displacement current which decays in time. If the relaxtion time is less than the transit time the current will settle to a plateau, otherwise the TOF signals will be dispersive. If carriers are injected into the occupational DOS, i.e. under conditons of quasi-equilibrium, no further relaxation occurs, i.e. the TOF signal will be flat until the carriers will recombine with the exit electrode. However, if carriers generated at an energy below ε_∞, the carriers have to be heat up via temperature and field assisted activation. Therefore, the current must increase prior to the transit time. Confirmation of this notion was provided by TOF experiments on a derivatized methylphenylmethane (MPMP) [80]. It turned out that cusps were observed upon photoinjection from α-selenium, yet not with a phenylene pigment, the distinguishing property being the energy level at which injection occurs. Monte Carlo simulation for injection into a Gaussian DOS as a function of the energy of the injection site were in accordance with experiment. They confirm that $\partial \ln j / \partial \ln t$ changes sign from negative to positive upon shifting of the energy of the site at which injection occurs towards lower energies. At the same time the carriers arrival time is virtually unaffected.

The present results support this notion. Upon photoexcitation within the excitonic $S_1 \leftarrow S_0$ absorption band geminate pairs are formed at the tails of the spectrum of transport sites because the energy of a singlet exciton is barely sufficient to generate a coulombicaly bound electron-hole pair and is, thus unable to undergo further relaxation[81]. A hole which can contributes to the photocurrent will therefore be strongly localized and needs thermal activation in order to contribute to the

photocurrent. The increase of the photocurrent prior to the transit time is a signature of this heating effect and has nothing to do with any possible distortion of the TOF-signals due to space charge effects. The effect becomes even more pronounced as the temperature increases because of the upward shift of the occupational DOS under condition of quasi-equilibrium is raised. The consequence is (i) the absence of dispersive transport for temperatures less than the critical temperature, defined by the condition $\sigma_c < 5.2$, and (ii) the evolution of a cusp of TOF signals at higher temperature and at high electric fields.

In the case of injection from a sensitizing layer the situation is different. Based upon the measured oxidation potential of PPV-ether, which is -0.92 V vs Ag/AgCl, the center of the hole transporting states, e.g. the HOMO, is at an energy -5.32 eV below vaccum. On the other hand, the center of the occupational density of hole states at a given field is at an energy $(\sigma^{eff})^2/kT$ above the center DOS. For $F = 5 \times 10^5$ V/cm and T = 293 K, $\sigma^{eff} \cong$ 50 meV and $\sigma^{eff}/kT \cong 0.1$ eV. This defines a demarcation energy of -5.2 eV for sensitized hole injection into PPV-ether, recalling that hole injection occurs from the HOMO level of an optically excited sensitizer. On the other hand the oxidation potential of rhodamine 6G is 1.23 V relative to SCE [82] implying that the HOMO level is at –5.7 ± 0.1 eV below the vacuum level. Therefore injection occurs far from quasi-equilibrium and the injected holes are liable to relaxation within the DOS. This explains why a transition from non-dispersive to dispersive transport can occur at lower temperatures. Therefore the occurrence of cusps in TOF-signals, unaffected by space charge distortion, is a signature of a memory effect as far as transport of charges injected into disordered systems is concerned.

5 Summary

In this chapter, the most crucial results of the thesis mainly from chapters 2, 3 and 4 are summarized. A German translation is also given at the end of this part.

5.1 English version

Stationary, as well as, time-resolved fluorescence studies as introduced in chapter 3 have provided a deep understanding of the excitation dynamics in phenyl substituted poly phenylenevinylene (PhPPV), which is a very promising material for commercial polymer LEDs. The analysis of the spectroscopic properties of PhPPV films doped with various amounts of an electron acceptor (trinitrofluorenone - TNF) allows not only to distinguish between energy transfer among segments of the polymer and dissociative quenching of singlet excitations. It is also possible to estimate the concentration of residual electron acceptors of either chemical or physical origin. These are responsible for the reduction of the fluorescence lifetime of PhPPV films (~ 400 ps) compared to solution (700 ps). The amount of electron acceptors turns out to be below 0.04 wt-% (400 ppm).

Furthermore, it has been clarified in chapter 4 whether singlet exciton quenching by those defects is the origin of photoconduction or not. In films of pure PhPPV and PhPPV doped with TNF spectral, field and temperature dependences of charge carrier photogeneration quantum yield were measured. One of the mechanisms by which charge carriers are produced was identified as surface sensitized extrinsic photogeneration in both doped and undoped films. These films were sandwiched between ITO and Al contacts with positively biased ITO. On the other hand, photocurrents observed in Al/PhPPV/Al samples revealed all characteristic features of intrinsic carrier photogeneration. It was found that doping with TNF facilitates the photoconductivity in PhPPV at relatively low excess photon energies. Although this effect is weak because of competitive photogeneration due to unidentified sensitizer present in neat samples. The field and temperature dependences of the dopant-assisted photogeneration are similar to those observed in intrinsic samples. A comparative analysis of the doping effects on the photoluminescence intensity and the photocurrent action spectra leads to the conclusion that the dissociation of primary optical excitations is the dominant mechanism of charge carrier photogeneration in both doped and intrinsic PhPPV at low excess photon energies above the $S_1 \leftarrow S_0$ transition. At higher excess photon energies intrinsic photogeneration occurs via on-chain dissociation of hot excitons.

From results of time-of-flight mobility experiments in chapter 5 it is obvious that in conjugated polymers charge carrier transport is conceptionally no different from that of low molecular glasses or molecularly doped polymers. Absolute values of the charge carrier mobility, for instance, typically about 5×10^{-4} cm^2/Vs at room temperature are comparable as are the functional dependencies of the mobility. It is remarkable that the

$T \rightarrow \infty$ intercept μ_0 of the $\mu(T)$ dependence of poly phenylenevinylene-ether (PPV-ether) is virtually the same as that of ladder type methyl substituted poly-paraphenylene (MeLPPP) and PAPPV, i.e. $\cong 3 \times 10^{-3}$ cm^2/Vs. On the other hand, the μ-values of molecularly doped polymers - at a level of doping on the order of 30 % - are about one order of magnitude higher. Since μ_0 is unaffected by any temperature dependent polaron effect, one has to conclude that, firstly, the rate controlling process is inter-site hopping and, secondly, the electronic overlap between the hopping sites must decrease in the series molecular crystal → molecularly doped polymer → conjugated polymer. One plausible reason may be related to the increasing charge delocalization as the π-electron systems get larger [83]. As a charge carrier is spread out inside a conjugated segment in a non-crystalline solid the inter-site transfer may be restricted by favorable inter-chain contacts. Therefore one loses rather than wins as far as charge motion is concerned when extending π-conjugation in a polymer.

5.2 Deutsche Version

Die Ergebnisse der in Kapitel 3 vorgestellten stationären sowie zeitabhängigen Fluoreszenzmessungen erlauben ein deutlich vertiefteres Verständnis der Anregungsdynamik in Phenyl substituierte Poly-Phenylvinylen (PhPPV), einem Material, das als sehr vielversprechend im Hinblick auf einen mögliche Einsatz in kommerziellen, organischen LEDs gilt. Durch die detaillierte Analyse der optischen Eigenschaften dünner PhPPV-Filme, dotiert mit verschiedenen Mengen eines Elektron-Akzeptors (Trinitrofluorenon - TNF), kann man nicht nur zwischen Energietransfer zwischen Polymersegmenten und der Fluoreszenzlöschung aufgrund der Dissoziation von Singulett-Exzitonen unterscheiden. Es ist vielmehr auch möglich eine Abschätzung über die Konzentration der verbliebenen Elektron-Akzeptoren zu geben, die sowohl chemischen als auch physikalischen Ursprungs sein können. Diese sind dafür verantwortlich, daß die Fluoreszenzlebensdauer in einem PhPPV-Film mit etwa 400 ps deutlich schneller ist als in der Lösung mit 700 ps. Die Konzentration liegt dabei unter 0.04 Gew.-% (400 ppm).

Weiterhin konnte geklärt werden in Kapitel 4 ob Singulett-Exziton-Löschung durch diese Defekte die Ursache der Photoleitung sein kann. Bei dünnen Filmen von reinem PhPPV sowie bei mit TNF dotierten PhPPV-Filmen wurden spektrale Abhängigkeit, Feldabhängigkeit und Temperaturabhängigkeit der Photoleitung gemessen. In beiden Fällen konnte oberflächeninduzierte, extrinsische Photogeneration als Ursache für die Ladungsträgergeneration ermittelt werden. Diese Filme befanden sich zwischen einem ITO und einem Al-Kontakt mit ITO als positiver Elektrode. Anderseits wiesen alle

Photoleitungsexperimente bei Proben der Kombination Al/PhPPV/Al die charakteristischen Signaturen intrinsischer Ladungsträgergeneration auf. Das dotieren mit TNF erleichtert die Photoleitung in PhPPV bereits bei relativ geringen Anregungsenergien. Allerdings ist dieser Effekt vergleichsweise gering, da gleichzeitig Photogeneration von Ladungsträgern durch nicht identifizierte Sensibilisatoren stattfindet. Die Feld- und Temperaturabhängigkeit der durch die Dotierung verbesserten Photogeneration sind ähnlich derer wie sie in reinen Filmen beobachtet werden. Eine Analyse der Dotierungseffekte auf die Photolumineszenzintensitäten sowie die Photoleitungsanregungsspektren führen zu der Schlußfolgerung, daß die Dissoziation vornehmlich optischer Anregungen der dominierende Mechanismus für die Ladungsträgergeneration sowohl in dotierten als auch reinen PhPPV-Filmen ist, solange man sich bei der Anregungsenergie nicht sehr weit oberhalb des $S_1 \leftarrow S_0$ – Übergangs befindet. Bei höheren Anregungsenergien findet intrinsische Photogeneration von Ladungsträgern durch Dissoziation „heißer“ Exzitonen auf der Polymerkette statt.

Die Resultate der Flugzeit (TOF) - Beweglichkeitsexperimente aus Kapitel 5 führen zu dem ziemlich eindeutigen Ergebnis, daß sich der Ladungsträgertransport in konjugierten Polymeren konzeptionell nicht von dem in molekularen Gläsern oder mit Molekülen dotierten Polymeren unterscheidet. Sowohl die absoluten Werte der Ladungsträger-beweglichkeiten, zum Beispiel, typischerweise ca. 5×10^{-4} cm^2/Vs bei Raumtemperatur als auch die ihre funktionellen Abhängigkeiten sind prinzipiell vergleichbar. Bemerkenswert ist, daß der Grenzwert der temperaturabhängigen Ladungsträger-beweglichkeit für $T \rightarrow \infty$ μ_0 bei Polyphenylenvinylen-Ether (PPV-ether) praktisch mit dem für MeLPPP und PAPPV übereinstimmt. Er liegt bei etwa 3×10^{-3} cm^2/Vs.

Anderseits sind die Ladungsträgerbeweglichkeiten bei mit Molekülen dotierten Polymeren – bei einem Dotierungsgrad von 30 % – etwa eine Größenordnung höher. Da μ_0 nicht von temperaturabhängigen Polaroneffekten beeinflußt wird, lassen sich daraus zwei Schlußfolgerungen ziehen: Erstens ist die ratenbestimmende Prozeß ein Hüpfprozeß zwischen Sites verschiedener Polymerketten (Inter-Site-Hüpfprozeß), zweitens muß sich der elektronische Überlapp zwischen den Hüpf-Sites von Molekülkristallen über moleküldotierte Polymeren hin zu konjugierten Polymeren verringern. Dies hat wahrscheinlich mit der vergrößerten Ladungsdelokalisation in ausgedehnteren π-Elektronensystem zusammenhängen [83]. Wenn ein Ladungsträger sich in einem konjugierten Segment eines nicht-kristallinen Festkörperpers befindet, kann sich der Inter-Site Ladungstransfer auf wenige, bevorzugte Interkettenkontakte reduzieren. Somit bedeutet die weitere Ausdehnung der π-Konjugation in einem Polymer einen Rückschritt im Hinblick auf die Bewegung der Ladungsträger.

6 Appendix

6.1 Abbreviations

a. u. : arbitrary units

CGL : charge generation layer

CTL : charge transport layer

DOS : density of states

e..h : electron and hole

E_{loc} : localization energy

EMA : effective medium approximation

GP : geminately bound e..h pair

GPC : gel permeation chromatography

HOMO : highest occupied molecular orbital

ITO : indium tin oxide

I_{ph} : photocurrent

LED : light-emitting diode

LUMO : lowest unoccupied molecular orbital

MDP : molecularly doped polymer

MeLPPP : ladder type methyl substituted poly-(para-phenylene)

MT : multiple trapping

NIR : near infrared

ODOS : occupied density of states

p.A. : pro analysis

PC : polycarbonate

PAPPV : poly(N-phenylimino-1,4-phenylene-1,2-ethenylene-2,5-dioctyl-1,4-phenylene-1,2-ethenylene-1,4-phenylene)

PhPPV : phenyle substituted poly-para-phenylenevinylene

PLE : photoluminescence excitation

PPV : poly-(para-phenylene-vinylene)

PVK : poly vinyl karbazol

SSA : singlet-singlet-annihilation

R6G : rhodamine 6G

TOF : time-of-flight

TTA : triplet-triplet-annihliation

UV : ultraviolet

VIS : visible

t_{Tr} : transit time

T_c : critical temperature

T_g : glass temperature

TRPL : time resolved photoluminescence

6.2 Friquently used units and constants

100 nm = 100×10^{-9} m = 10^{-7} m = 10^{-5} cm = 1 kÅ

W = AV, J = AVs = Ws = (C/s)Vs = CV, $hc / \lambda = hv$

where h (Planck's constant) = 6.62618×10^{-34} Js

e (elementary charge) = 1.60219×10^{-19} C

c (speed of light in vacuum) = 2.997925×10^{8} m/s

Converting example

c / 560 nm = 5.4×10^{14} Hz

1239.85×400 nm = 3.1 eV

Unit converting for charge carrier photogeneration quantum yield

$$\varphi_{ph} = \frac{I_{ph}(A) \cdot h\nu(Js \cdot s^{-1})}{P_{lamp}(W) \cdot n_{abs} \cdot e(C)}$$

$$N_{abs.ph} = \frac{P_{lamp} \cdot n_{abs}}{h\nu} = \frac{AV}{Js \cdot s^{-1}} = \frac{AV}{AVs} = s^{-1}, \quad N_{ch} = \frac{I_{ph}}{e} = \frac{A}{C} = \frac{Cs^{-1}}{C} = s^{-1}$$

6.3 References

1. Hermann Hesse, “Demian” (1917)
2. J.H. Burroughes, D.D.C. Bradley, A.R. Brown, R.N. Marks, K. Mackay, R.H. Friend, P.L. Burn, and A.B. Homes, Nature, **347**, 539 (1990)
3. R.H. Fiend, R.W. Gymer, A.B. Holmes, J.H. Burroughes, R.N. Marks, C. Taliani, D.D.C. Bradley, D.A. Dossantos, J.L. Bredas, M. Logdlund, and W.R. Salaneck, Nature, **397**, 121 (1999)
4. H. Sirringhaus, N. Tessler and R.H. Friend, Science, **280**, 1741 (1998)
5. J.J.M. Halls, C.A. Walsh, N.C. Greenham, E.A. Marseglia, R.H. Friend, S.C. Moratti, and A.B. Holmes, Nature, **376**, 498 (1995)
6. R.E. Peierls, Quantum Theory of Solids, Oxford (1995)
7. W. P. Su, J. R. Schrieffer, and A. J. Heeger, *Phys. Rev. Lett.* **42,** 1698 (1979)
8. J. Heeger, S. Kivelson, R. J. Schrieffer, and W. P. Su, *Rev. Mod. Phys.* **60,** 782 (1988)
9. D. Moses, A. Dogariu, and A.J. Heeger, *Phys. Rev. B*, **61**, 9373 (2000)
10. H. Bässler in Primary Photoexcitations in Conjugated Polymers: Molecular Exciton versus Semiconductor Band Model, edited by N.S. Sariciftci (World Scientific, Singapore, 1997)
11. U. Rauscher, H. Bässler, D. D. C. Bradley, and M. Hennecke, *Phys. Rev. B*, **42,** 9830 (1990)
12. S. Heun, R. F. Mahrt, A. Greiner, U. Lemmer, H. Bässler, D. A. Halliday, D. D. C. Bradley, P. L. Burn, and A. B. Holmes, *J. Phys. Condens. Matter*., **5,** 247 (1993)

13. M. C. J. M. Vissenberg and M. J. M. de Jong, *Phys. Rev. Lett.*, **77,** 4820 (1996)
14. V. I. Arkhipov, E. V. Emelianova, and H. Bässler, *Phys. Rev. Lett.*, **82,** 1321 (1999)
15. D. J. Pinner, R. H. Friend, and N. Tessler, J. Appl. Phys., **86**, 5116 (1999)
16. P. W. M. Blom and M. C. J. M Vissenberg, Mater. Sci., **27**, 53 (2000)
17. P. K. H. Ho, J. S. Kim, J. H. Burroughes, H. Becker, S. F. Y. Li, M. Brown, F. Cacialli, and R. H. Friend, Nature, **404**, 481 (2000)
18. J. M. Lupton, B. J. Matterson, I. D. W. Samuel, M. J. Jory, and W. L. Barnes, Appl. Phys. Lett. **77**, 3340 (2000)
19. U. Lemmer, R. F. Mahrt, Y. Wada, A. Greiner, H. Bässler, and E. O. Göbel, Appl. Phys. Lett. **62**, 2827 (1993)
20. P. Schouwink, G. Gadret, and R. F. Mahrt, Chem. Phys. Lett. **341**, 213 (2001)
21. P. Monkman, H. D. Burrow, I. Hamblett, S. Navaratnam, U. Scherf and C. Schmitt, *Chem. Phys. Lett.*, **327**, 111 (2000)
22. H. Bässler, D. Hertel, S. Setayash, H. G. Nothofer, U. Scherf and K. Müllen, *Adv. Mater.*, **13**, 65 (2001)
23. M.G. Harrison, S. Möller, G. Weiser, G. Urbasch, R. F. Mahrt and H. Bässler, *Phys. Rev. B*, **60**, 8650 (1999)
24. J. Rissler, H. Bässler, F, Gebhard and P. Schwerdtfeger, *Phys. Rev. B*, **64**, 645122 (2001)
25. A. Horvath, G. Weiser, G. L. Baker and S. Etemad, *Phys. Rev. B*, **51**, 2751 (1995)
26. S. F. Alvarado, P. F. Seidler, D. G. Lidzey and D. D. C. Bradley, *Phys. Rev. Lett.*, **81**, 1082 (1998)

27. L. Rossi, S. F. Alvarado, W. Riess, S. Schrader, D. G. Lidzey and D. D. C. Bradley, *Synth. Met.*, **111**, 527 (2000)

28. J. Opfermann, H. H. Hörhold, *Z. Phys. Chem*.(Leipzig), **259**, 1089 (1978)

29. S. Barth, H. Bässler, U. Scherf, and K. Müllen, Chem. Phys. Lett. **288,** 147 (1998)

30. M. Chandross, S. Mazumdar, S. Jeghinski, X. Wei, Z.V. Vardeny, E. W. Kwock and T. Miller, *Phys. Rev. B*, **50**, 14702 (1994)

31. T. K. Däubler, V. Cimrova, V. Pfeiffer, H. H. Hörhold and D. Neka, *Adv. Mater.*, **11**, 1274 (1999)

32. D. Hertel, H. Bässler, S. Möller, H. Tilmann and H. H. Hörhold, *Mol. Cryst. Liq. Cryst.*, **355**, 175 (2001)

33. T. Ueda, R. Fujisawa, H. Fukumura, A. Itaya, and H. Masuhara, *J. Phys. Chem*., **99**, 3629 (1995)

34. V.R. Nikitenko, Y.H. Tak and H. Bässler, J. Appl. Phys., **84**, 2334 (1998)

35. H. Bässler, phys. stat. sol. (b) **175**, 15 (1993)

36. L. Kador, J. Chem. Phys., **95**, 5574 (1991)

37. P.M. Borsenberger and D.S. Weiss, Organic Photoreceptors for Xeroxgraphy, Marcel Dekker, New York, 1998

38. H. Bässler, in Electronic Materials: The Oligomer Approach, ed. by K. Müllen and G. Wegner, Wiley-VCH, Weinheim, 1998, p. 403

39. H. Meyer, D. Haarer, H. Naarmann, and H.H. Hörhold, Phys. Rev. B, **52**, 2587 (1995)

40. R.F. Mahrt, T. Pauck, U. Siegner, M. Hopmeier, R. Hennig, H. Bässler, and E.O. Göbel, Phys. Rev. B, **54**, 1759 (1996)

41. D. Hertel, U. Scherf, and H. Bässler, Adv. Mat., **10**, 1119 (1998)

42. D. Hertel, H. Bässler, U. Scherf, and H.H. Hörhold, J. Chem. Phys., **110**, 9214 (1999)

43. M. Gailberger, and H. Bässler, Phys. Rev. B, **44**, 8643 (1991)

44. H. Bässler, in Semiconducting Polymers, ed by G. Hadziioannou and P.H. van Hutten, Wiley-VCH, Weinheim, 2000, p. 365

45. M. Redecker, D.D.C. Bradley, M. Inbasekaran, W.W.Wu, and E.P.Woo, Adv. Mat. **11**, 214 (1999)

46. M. Redecker, D.D.C. Bradley, M. Jandke and P. Strohriegl, Appl. Phys. Lett., **75**, 109 (1999)

47. H. Becker, H. Spreitzer, W. Kreuder, E. Kluge, H. Schenk, I. Parker, and Y. Cao, Adv. Mater. **12**, 42 (2000)

48. H. Spreitzer, W. Kreuder, H. Becker, H. Schenk, N. Yu, *PCT Patent Application WO99/24526*, **1997**

49. S. Heun, R. F. Mahrt, A. Greiner, U. Lemmer, H. Bässler, D. A. Halliday, D. D. C. Bradley, P. L. Burn and A.B. Holmes, J. Phys. Condens. Matter, **5**, 247 (1993)

50. D. W. Samuel, G. R. Rumbles and A. J. Collison, Phys. Rev. B, **52**, 11573 (1995)

51. R. I. Personov, in Spectroscopy and Excitation Dynamics of Condensed Molecular Systems, V. M. Agranovich and R. M. Hochstrasser (edi.), North Holland, Amsterdam, p. 535 (1983)

52. B. Mollay, U. Lemmer, R. Kersting, R. F. Mahrt, H. Kurz, H. F. Kauffmann, H. Bässler, Phys. Rev. B **50**, 10769, 1994

53. B. Berlman, in Handbook of Fluorescence Spectra of Aromatic Molecules, second. ed., Academic Press, New York and London, p. 15 (1971)

54. T. Ueda, R. Fujisawa, H. Fukumura, A. Itaya, and H. Masuhara, J. Phys. Chem., **99**, 3629 (1995)

55. J. Klafter and A. Blumen, Chem. Phys. Lett, **119**, 377 (1985)

56. A. Kadashchuk, Yu. Skryshevskii, A. Vakhnin, N. Ostopenko, V. I. Arkhipov, E. V. Emelianova and H. Bässler, Phys. Rev. B, **63**, 115205 (2001)

57. R. Richert and H. Bässler, J. Chem. Phys., **84,** 3567 (1986)

58. K. Brunner, A. Tortschanoft, Ch. Warmuth, H. Bässler and H. F. Kauffmann, J. Phys. Chem. B, **104**, 3781 (2000)

59. R. F. Mahrt, T. Pauck, U. Lemmer, U. Siegner, M. Hopmeier, R. Hennig, H. Bässler and E. O. Göbel, Phys. Rev. B, **54**, 1759 (1996)

60. B. Movaghar, M. Grünewald, B. Ries, H. Bässler and D. Wuertz, Phys. Rev. B, **33**, 5545 (1986)

61. R. Kersting, U. Lemmer, M. Deussen, H. J. Bakker, R. F. Mahrt, H. Kurz, V. I. Arkhipov, H. Bässler, and E. O. Göbel, *Phys. Rev. Lett.*, **73,** 1440 (1994)

62. V. I. Arkhipov, H. Bässler, M. Deussen, E. O. Göbel, R. Kersting, H. Kurz, U. Lemmer, and R. F. Mahrt, *Phys. Rev. B*, **52,** 4932 (1995)

63. H. Becker, H. Spreitzer, W. Kreuder, E. Kluge, H. Schenk, I. Parker, and Y. Cao, *Adv. Mater*., **12,** 42 (2000)

64. C. Im, J. Lupton, P. Schouwink, S. Heun, H. Becker and H. Bässler, *J. Chem. Phys*., 22. April 2002, accepted.

65. G. Vaubel, H. Bässler and D. Möbius, *Chem. Phys. Lett.*, **10**, 334 (1971)

66. B. Schweitzer, V. I. Arkhipov, U. Scherf, and H. Bässler, *Chem. Phys. Lett*., **313,** 57 (1999)

67. J.-W. van der Horst, P. A. Bobbert, M. A. J. Michels and H. Bässler, *J. Chem. Phys*., **114**, 6950 (2001)

68. A. Kadashchuk, Yu. Skyshevskii, A. Vakhnin, N. Ostaperrko, V. I. Arkhipov, E. V. Emelianova and H. Bässler, *Phys. Rev. B*, **63**, 115205-1 (2001)

69. U. Albrecht and H. Bässler, *Phys. stat. sol. (b)*, **191**, 455 (1995)

70. V. I. Arkhipov, E. V. Emelianova, and H. Bässler, *Chem. Phys. Lett*., **296,** 452 (1998)

71. V. I. Arkhipov, E. V. Emelianova, S. Barth, and H. Bässler, *Phys. Rev. B*, **61**, 8207 (2000)

72. A. Hirao, T. Tsukamoto, and H. Nishizawa, Phys. Rev. B, **59**, 12991 (1999)

73. W.G. Gill, J. Appl. Phys., **43**, 5033 (1972)

74. P.M. Borsenberger, L. Pautmeier, and H. Bässler, J. Chem. Phys., **94**, 5447 (1991)

75. D.H. Dunlap, P.E. Parris, and V.M. Kenkre, Phys. Rev. Lett., **77**, 542 (1996)

76. S.V. Novikov, D.H. Dunlap, V.M. Kenkre, P.E. Parris, and A.V. Vannikov, Phys. Rev. Lett., **81**, 4472 (1998)

77. J.A. Sinicropi, J.R. Cowdery-Corvan, E.H. Magin, and P.M. Borsenberger, Chem. Phys., **218**, 331 (1997)

78. M. Novo, M. van der Auweraer, F.C. de Schryver, P. Borsenberger, and H. Bässler, phys. stat. sol. (b), **177**, 223 (1993)

79. A. Ochse, A. Kettner, J. Kopitzke, J.-H. Wendorff, and H. Bässler, Phys. Chem. Chem. Phys. **1**, 1757 (1999)

80. P.M. Borsenberger, L. Pautmeier, and H. Bässler, J. Chem. Phys., **95**, 1258 (1991)

81. B. Schweitzer and H. Bässler, Synth. Met., in press

82. S.M. Park, A.J. Bard, J. Electroanal. Chem. Interfacial Electrochem. **77**, 137 (1977)

83. M. Knupfer, T. Pichler, M.S. Golden, and J. Fink, M. Murgia, R.H. Michel, R. Zamboni, and C. Taliani, Phys. Rev. Lett., **83**, 1443 (1999)

6.4 Dankesagung

An dieser Stelle möchte ich herzlich danken:

- Herrn Prof. Dr. H. Bässler für die interessante Themenstellung, seine ständige Bereitschaft zu hilfreichen Diskussionen.
- Herrn Prof. Dr. J. H. Wendorff für die Bereitschaft zur Erstellung des Zweitgutachtens.
- Herrn Prof. V. Arkhipov und seine ehemalige Mitarbeiterin Frau Dr. E.V. Emelianova, und Herrn Dr. V. Nikitenko für die wertvollen Diskussionen.
- Herrn Prof. Dr. H.H. Hörhold und seinen Mitarbeitern für die Herstellung von PPV-Ether.
- Herrn Dr. H. Vestweber, Frau Dr. S. Heun, Herrn Dr. H. Spreitzer und Herrn Dr. H. Becker für die Bereistellung von Super Yellow PPV.
- Herrn Dr. S. Barth für die Einführung in die organische Optoelektronik.
- Herrn Dr. Klaus Book, Herrn Dr. Dirk Hertel, Frau Dipl.-Chem. Anja Gehard, Frau Dipl.-Chem. Anna Hayer, Herrn Dr. Christian Bauer, Herrn Dr. Jörg Rissler, Herrn Dipl.-Chem. Oliver Narwark, Herrn Dr. Stefan Meskers, Frau Dr. Wenjing Tian, Herrn Dr. Yura Romanovskii und allen anderen Mitgliedern der Arbeitsgruppe für das gute Arbeitsklima, die ständige Hilfs- und Gesprächsbereitschaft.
- Frau H. Rothe für die Bereitstellung des Laborbedarfs.
- Herrn Dr. J. Lupton und Herrn Dr. P. Schouwink für die Hilfe bei den Streak Camera-Messungen.
- Herrn Dr. M. Rahn und Herrn Dr. D. West für das Super TNF.
- Herrn Dr. W. Stolz für die Zurverfügungstellung der spin-coating-Anlage.
- Herrn W. Kröschel und seinen Mitarbeiter der Elektronik-Werkstatt für die Unterstützung bei der Lösung diverser elektronischer Probleme.
- Herrn A. Schirrmeister und allen Angestellten der Feinmechanik-Werkstatt.
- Herrn R. Donner und Frau E. Waschk für die große Hilfe bei vielen bürokratischen Schwierigkeiten.

Und natürlich all denen, die ich hier vergessen haben sollte.